COMPOSITION-STRUCTURE-PROPERTY RELATIONSHIPS IN MAGNESIUM YTTRIUM ALUMINOBORATE GLASSES

by

ANNE ELISABETH REBECCA

A thesis submitted to the

School of Graduate Studies

Rutgers, The State University of New Jersey

In partial fulfillment of the requirements

For the degree of

Master of Science

Graduate Program in Materials Science and Engineering

Written under the direction of

Ashutosh Goel

And approved by

_____

_____

_____

New Brunswick, New Jersey

January 2019

ABSTRACT OF THE THESIS

Composition-structure-property Relationships in Magnesium Yttrium Aluminoborate Glasses

by ANNE ELISABETH REBECCA

Thesis Director:

Ashutosh Goel

There is an increasing need for light-weight, strong and crack-resistant glasses for industrial applications. In order to design new glasses, a thorough understanding of relationships between composition, structure, and properties is required. This study attempts to shed more light on the composition-structure-property relationships in alumina-rich aluminoborate glasses. In the present work, MgO-Y_2O_3-Al_2O_3-B_2O_3 glasses have been fabricated by melt-quenching at temperatures ranging from 1600°C to 1650°C. The influence of the substitution of B_2O_3 by Al_2O_3 on the structure, thermal and mechanical properties of the glasses (hardness and crack resistance) have been investigated using magic angle spinning – nuclear magnetic resonance (MAS-NMR), differential scanning calorimetry (DSC) and Vickers indentation. Hardness and crack resistance of the glasses were found to correlate with their structure and composition. Furthermore, with Al_2O_3/B_2O_3 substitution, fragility, density and hardness were found to increase while glass forming ability as well as crack resistance decreased.

Acknowledgements

I would like to thank first my advisor and professor, Dr. Ashutosh Goel, for his guidance and presence during the duration of this project. It has been one of the most interesting experiences in my life, being his student, learning and growing under his supervision. His work ethics, attitude, and passion towards advancing knowledge in this field are commendable. Thank you, Dr. Goel, for the past two years spent as a member of your group. I would like to thank my other thesis committee members: Drs. Koray Akdogan and Richard Lehman. Thank you for taking the time to read my thesis and agreeing to be part of my defense committee. Thank you also for teaching and passing along knowledge that I have used in the past and will use in the future.

I want to also to thank Dr. Saurabh Kapoor for being an invaluable help along the road. Your questions, answers, insights have proven extremely helpful during this journey. Thank you for making your knowledge and skills available to me and this work for the past year. I want to extend my gratitude as well to Dr. Smedjskaer and his student Kacper Januchta at Aalborg University, J. Klotz, B. Rice and R. Youngman from Corning Inc.

Thank you to the department of Materials Science and Engineering of Rutgers University. The members of this department have been most helpful and always make themselves available to help others. Thank you to Dr. Lehman for being the chair of this department and making sure we have events that help us display our research and interest to external students, helping to expand our experiences beyond our coursework and our projects. Thank you to Dr. Robert Horvath for being always so helpful in the lab and supervising our glass melting demos anytime we have them. Thank you to Sheela Sekhar

and Nahed Assal for making themselves available to answer any questions we have, especially at the beginning of each semester.

I would like to thank my group members: past and present. Thank you, guys, for being of help generally in the lab and special thanks to Nick for running some of the NMR measurements for my samples. Thanks to all of you for the movie nights, impromptu lunches, dinners, get-togethers. Those have been nice bonding experiences that have made the challenges I have come across easier to overcome. Thank you, guys, for the serious times and the fun times.

Finally, thank you to the sponsor that has made this project possible. Thank you to British Aerospace Engineering (BAE) for providing the money to work on this project. Thank you to Dr. Vic Kelsey for his vested interest in this project and inputs. Thank you to Dr. Richard Haber of the Ceramic, Composite and Optical Materials Center (CCOMC) for his inputs as well these past couple of years. This work was made possible through funding from NSF Grant No.1507131.

Dedication

I would like to dedicate this thesis to my family and closest friends. This would not be possible without them. Thank you so much for being there for me since the beginning, and even more so these past couple of months. Special thanks to my mother for offering her ever-present shoulder to lean on for emotional support, my sister and her husband for their support as well and rides to/from campus whenever I needed them, especially on weekends. Special thanks as well to my brothers for helping me see the bright side of things, for making me laugh until I cry and for driving me as well when I needed it. Thank you, Kendy, for your patience and your encouragements, the late nights spent listening to me. Thank you for being so interested in what I was doing and asking questions. Your support was unconditional and there are no words to adequately convey how grateful I am to you guys.

Preface

The inductively coupled plasma – mass spectroscopy (ICP-MS) measurements were conducted at Corning Inc. by B. Rice and J. Klotz.

The elastic properties measurements data was supplied by M. Smedjskaer and his student K. Januchta from Aalborg University in Denmark.

Part of this work has been presented at the 2018 Glass and Optical Materials Division (GOMD) conference.

Table of Contents

Abstract ii

Acknowledgements iii

Dedication v

Preface vi

Table of Contents vii

Table of Figures ix

List of Tables x

Chapter 1 – Introduction 1

1.1 – Motivation 1

1.2 – Background 2

1.3 – Outline and Objectives 4

Chapter 2 – Literature Review 6

2.1 – Al_2O_3 in glasses 6

2.2 – B_2O_3 in glasses 7

2.3 – Aluminoborate glasses 8

2.4 – Structure and hardness 9

2.5 – Structure and crack resistance 12

Chapter 3 – Experimental Approach 16

3.1 – Design 16

3.2 – Synthesis 18

3.3 – Characterization 19

4 – Results and discussion 24

4.1 – Glass formation 24

4.2 – Thermal parameters and stability 25

4.3 – Structural characterization 30

4.4 – Density and hardness 34

4.5 – Crack resistance 37

Chapter 5 – Conclusions 40

Chapter 6 – Limitations and Future Work 41

6.1 – Ballistics test 41

6.2 – Composition stabilization 41

6.3 – Physical properties and chemical durability studies 42

6.4 – Further RE-aluminoborate compositions exploration 43

Chapter 7 – Supplementary results 44

7.1 – Plots for determination of activation energies 44

7.2 – Brillouin spectroscopy 45

References 47

Table of Figures

Figure 1: Hardness versus Al_2O_3 content for various classes of materials. Figure is copied from Rosenflanz et al.[10] 10

Figure 2: Different deformation mechanisms that can take place in a glass. Figure copied from original work[61]. 13

Figure 3: Diagram of Y_2O_3-Al_2O_3-B_2O_3 series compositions synthesized by Rutz et al.[54] as reproduced from original work. 17

Figure 4: Monolithic piece of Al-35 (MgO-Y_2O_3-Al_2O_3-B_2O_3) as-synthesized after annealing. 19

Figure 5: XRD of glasses, showing amorphous behavior. Only broad features can be observed on the spectra. 24

Figure 6: Curves of heat flow (mW/mg) versus temperature (°C) for series at a rate of 30°C/min in N2 atmosphere. 26

Figure 7: 11B MAS NMR spectra for glasses. 32

Figure 8: 27Al MAS NMR spectra for glasses. 32

Figure 9: Microindentation of Al-35 at various loads ranging from 100 gf. to 2000 gf. Figure is not drawn to scale. 35

Figure 10: Crack probability versus Al_2O_3 content in glass at 2000 gf. 37

Figure 11: Scaled up piece of Al-35 glass for ballistics impact response tests. Inhomogeneities can be observed in the glass due to the small forming region in this glass family and scaling up the composition. 41

List of Tables

Table 1: Compositions investigated in present study with values in mol.% Glasses are designated by their Al_2O_3 content. 18

Table 2: Difference in mol. % between experimental and batched compositions as determined by ICP-MS for two batches synthesized slightly differently: one batch melted for 2 hours and one batch re-melted for approximately 3 hours. 23

Table 3: Thermal parameters (glass transition temperature (T_g), onset of crystallization (T_c), crystallization temperature (T_p), and melting temperature (T_m) as determined by DSC measurements for a rate of 30°C /min in N_2 atmosphere. 25

Table 4: Stability indices (thermal stability (ΔT), Hruby parameter (K_H), fragility index (F) and activation energies associated with structural relaxation (E_{relax}), viscous flow (E_η), crystallization (E_c) for series. 29

Table 5: Boron and aluminum fraction for different coordination for glass series. $B^{[3]}$ is mainly present while there are significant amounts of $Al^{[5]}$. 31

Table 6: Glass transition temperature (T_g), density (ρ), atomic packing density (C_g), microhardness (H_v) and crack probability (%) at 2000 gf. for series. 34

Table 7: Young's modulus (E), shear modulus (G), bulk modulus (B) and Poisson's ratio (ν) for Al-35. 46

Chapter 1 – Introduction

"A glass can be defined as an amorphous solid completely lacking in long range, periodic atomic structure, and exhibiting a region of glass transformation behavior. Any material, inorganic, organic, or metallic formed by any technique, which exhibits glass transformation behavior is considered to be a glass."
Shelby JE. Introduction to Glass Science and Technology: Edition 2. 2005.

1.1 – Motivation

Glass is a universal material used in various industries such as automotive, electronics, and defense owing to its favorable properties such as high hardness as well as its transparency to visible light. Furthermore, the major advantage of glasses and glass-ceramics among their ceramic counterparts is their ability to accommodate various functional ions in their amorphous or crystalline phase, thus providing the flexibility to tailor and optimize their compositions with respect to different technological applications. However, glass is inherently brittle in nature and exhibits a low practical strength due the presence of minor flaws on its surface, which severely limits its applicability in various advanced applications[1]. Thus, any impact or scratch event leading to formation of cracks amplify local tensile stresses, resulting in catastrophic failures[1]. Therefore, increasing the hardness and crack resistance of glasses is critical for the development of scratch-resistant and mechanically durable glasses for advanced technological applications.

Traditionally, glasses have been treated by the application of chemical strengthening and thermal tempering to increase their hardness and crack resistance[2]. However, these are expensive and time-consuming post processing techniques[3]. In contrast, less attention has been paid towards understanding the composition-structure-property relationships in glasses. Therefore, in order to enable the design of new glass

compositions with improved properties, it is of paramount importance to understand the influence of composition on the structure and mechanical behavior of glasses.

In recent studies, alumina-rich glasses prepared using techniques such as aerodynamic levitation have shown excellent mechanical properties in terms of hardness and crack resistance[4]. However, using such methods, relatively small sample specimens (~ mm^2) are obtained, whereas, characterizing the glasses for industrially relevant properties requires larger samples (~ cm^2). Hence, there is a need to design glasses having high hardness and crack resistance with feasible processing parameters given the increasing demand for stronger, lighter, and crack resistant glasses. Therefore, this work aims to develop alumina-rich oxide glasses with good mechanical properties and to understand their composition-structure-property relationships, which could eventually widen the scope of applications glasses could be used for.

1.2 – Background

According to Griffith's criterion of failure, introduction of a flaw to the surface of a glass weakens its strength significantly[1], with crack initiation and subsequent propagation playing their roles into weakening the material[1]. In addition to it, Griffith inferred that the strength of glass depends on the size of critical defects present, thereby suggesting that the inherent strength of glass is several orders of magnitude higher than the empirical strength. Hence the theoretical strength of glass is quite high, ranging from 10 to 30 GPa from various early calculations[1, 5, 6]. However, glasses have been observed to withstand only low levels of tensile stresses because of its inherent brittleness, which limits its applications[2]. Therefore, different methods have been used and are currently

used to improve the resistance of glass to surface damage[2, 3, 7-9]. The current generation of commercial glasses undergo post-synthesis treatments like chemical strengthening (i.e. ion-exchange), physical strengthening (i.e. thermal tempering), or application of compressive coatings to improve the mechanical durability[2]. However, these techniques have a limited scope of applications due to cost and practicability[3]. For example, ion-exchange is an expensive process while thermal tempering is effective only for certain shapes and thicknesses[3]. Due to this reason, the last few years have witnessed a consistent upsurge in the studies aiming to improve the inherent mechanical properties of glasses by compositional tuning[4, 10-14].

Alumina (Al_2O_3)-rich oxide glasses are potential candidates for cover glass and armor applications due to their high hardness, elastic modulus and bond strength[15, 16]. Al_2O_3 is a high melting temperature metal oxide (>2000°C) with a poor glass forming ability[17]. Exceedingly high cooling rates, estimated to be in orders of magnitude up to 10^7 K/s are required to cool Al_2O_3 melts in order to avoid devitrification[17]. However, the required cooling rate can be lowered to the order of 10^3 K/s by mixing Al_2O_3 with other oxides. As a result, Al_2O_3 has been usually used in conjunction with oxides such as SiO_2, B_2O_3, CaO, RE_2O_3 (where RE = rare-earth) to increase its glass-forming ability[4, 10, 14, 18-22]. For example, rare-earth oxides and calcium oxide have been used in several studies to make binary Al_2O_3 glasses such as La_2O_3-Al_2O_3, Y_2O_3-Al_2O_3, Er_2O_3-Al_2O_3, CaO-Al_2O_3[10, 18]. Some of the glasses in the systems previously mentioned have shown hardness values as high as 9.5 GPa[10, 14], largely surpassing the observed hardness (5 to 6.5 GPa) for industrially relevant alkali-alkaline-silicates and aluminosilicates [23-25,26]. However, synthesis of glasses with high Al_2O_3 content (>35 mol.%) is extremely

challenging using melt-quenching due to the high melting temperatures (>1800°C) required to synthesize these glasses as well as their low glass forming ability[10, 17, 18, 20, 21]. Methods such as aerodynamic levitation and flame-synthesis are employed for the synthesis [4, 10, 14], but the resulting products are in the sub-centimeter range in size which makes the scale up for commercial and industrial purposes problematic[10, 18, 20, 21]. As a result, it can be difficult to characterize the properties these glasses for industrial relevant applications, such as ballistics impact testing for armor applications[27].

Owing to the above-mentioned perspective it is of paramount importance to design and synthesize alumina-rich glasses using industrially feasible techniques such as melt quenching. Further, given the difficulties associated with synthesizing these glasses, our understanding of the composition-structure-property relationships of alumina-rich aluminoborate glasses is relatively poor[10]. Thus, the aim of the present study is to elucidate the influence of composition on the structure, and micromechanical properties (hardness and crack resistance) of Al_2O_3-rich MgO-Y_2O_3-Al_2O_3-B_2O_3 glasses with varying Al_2O_3/B_2O_3 ratio. By varying Al_2O_3/B_2O_3 ratio, we explore the influence of high field cations on the structure of aluminum and boron and on the mixing of the different network constituents. The structural changes as a function of composition are investigated using ^{11}B, and ^{27}Al MAS-NMR, whereas the micromechanical properties are investigated using Vickers indentation.

1.3 – Outline and Objectives

In the present work we have tried to synthesize glass compositions with high Al_2O_3 content and to understand the influence of composition on the structure, and

micromechanical properties (hardness and crack resistance) Al_2O_3-rich MgO-Y_2O_3-Al_2O_3-B_2O_3 glasses. The first chapter, i.e., the introduction, provides an outlook of the work carried out in the present thesis; the second chapter will focus a detailed literature review in the field of oxide mechanical properties of oxide glasses, with special emphasis on the Al_2O_3-rich oxide glasses. The third chapter deals with the description of the general experimental procedures and methodologies used along the thesis. It provides details about all the experimental techniques and procedures employed in order to synthesize, characterize, and test our samples. Chapter four is the most important part of this work as it presents all the experimental results obtained Al_2O_3-rich MgO-Y_2O_3-Al_2O_3-B_2O_3 glasses along with the pertaining discussions. In chapter five we have tried to conclude all the results and achievements obtained during this work and chapter six provides future directions in this field of research. Several experimental techniques were used throughout this investigation aiming at a better understanding of the glass structure, and micromechanical properties of the Al_2O_3-rich MgO-Y_2O_3-Al_2O_3-B_2O_3 glasses. Accordingly, the work reported in this thesis has been directed towards fulfilment of the following aims:

- To synthesize alumina rich glasses at low temperatures (<1650°C) in conventional laboratory furnaces.
- To investigate the influence of incorporation of Al_2O_3 on the glass forming ability of the aluminoborate glasses prepared using melt quenching technique.
- To conduct different characterization techniques including thermal characterization and mechanical characterization in order to understand different composition-structure-property relationships that govern these glasses.

Chapter 2 – Literature Review

2.1 – Al_2O_3 in glasses

Oxide glasses are classified into three different categories: network formers, network modifiers and network intermediates. Network formers are oxides that can form glasses without the assistance of other oxides. Network modifiers alter the glass structure by turning bridging oxygens (BO's) (predominantly covalent in character) into non-bridging oxygens (NBO's) (Si–O–M^+) linkages, predominantly ionic in character, where M^+ is a modifier cation. Lastly, network intermediates are oxides that can act as network formers under certain conditions and network modifiers under others[2]. As a network intermediate, while by itself Al_2O_3 will not form a glass, it will act as a network former in certain proportions with certain other oxides[28]. In other cases, it acts as a network modifier[29].

Al_2O_3 can exist in glasses in three different coordination species with oxygen: tetrahedral ($Al^{[4]}$), pentahedral ($Al^{[5]}$) and octahedral ($Al^{[6]}$) units. In simple ternary alkali/alkaline-earth aluminosilicates systems where the total concentration of Al_2O_3 is less than the total concentration of modifier content (per-alkaline), Al_2O_3 exists mostly in tetrahedral units. Addition of Al_2O_3 to aluminosilicate glasses increases the connectivity of the network by using the modifier cation for charge compensation. In cases where the ratio of alkali/alkaline-earth oxide to alumina is 1 (meta-aluminous), the alkali and alkaline-earth cations no longer play a role into creating NBO's and are used exclusively for charge compensation of $Al^{[4]}$ tetrahedra. In the compositional regime where the ratio of total modifier content to alumina content is less than 1 (per-aluminous), the structure exhibits significant fractions of Al in 5- and 6- coordination. In the case of high field

strength (ratio of charge to ionic radius) cation modifiers or the case where the concentration of Al_2O_3 far exceeds that of the modifier, alumina exists in $Al^{[4]}$ units along with significant fraction higher coordinated units, $Al^{[5]}$ and $Al^{[6]}$.

2.2 – B_2O_3 in glasses

B_2O_3 is a network former that can exist as either trigonal ($B^{[3]}$) or tetrahedral ($B^{[4]}$) units in the glass structure. Boron oxide readily changes its structure with composition, which in turn, affects various properties of the glass such as its glass transition temperature, melting point, viscosity etc[2]. The structure of amorphous B_2O_3 glasses has been shown to be composed of boroxol rings consisting of trigonal $B^{[3]}$ units[2]. In the presence of network modifying cations, boron undergoes a change in coordination[2]. At low modifier contents, the addition of network modifiers leads to the formation of $B^{[4]}$ units. These $B^{[4]}$ units are subsequently charge-compensated by the modifier cations. On the other hand, at high modifier contents, NBOs are formed along with the decrease in $B^{[4]}$ units. In addition, modifying cations with high field strength result in creation of higher number of NBOs in comparison to low field cations[30-33].

B_2O_3 is mostly used in conjunction with silica (borosilicate glasses) and/or alumina (aluminoborosilicate or aluminoborate glasses) in most commercial applications[2]. Unary borate glass, although possessing the highest glass formation tendency, is hygroscopic, which imposes limitations on its uses in technological applications[34, 35]. Borosilicate glasses, on the other hand, are resistant to chemical attack and thermal shock due to their low coefficients of thermal expansion. They have been used expansively in applications such as laboratory glassware and cookware[36].

Aluminoborate glasses themselves have seen uses in applications as sealing glasses[36]. In recent years, significant work has been carried out on understanding the structural basis of the chemical and mechanical properties of aluminoborate glasses[11, 29, 37-44].

2.3 – Aluminoborate glasses

In aluminoborate glasses, the structure of the glasses is partly dependent on the ratio of Al_2O_3 to B_2O_3. With the substitution of B_2O_3 by Al_2O_3, Al_2O_3 suppresses $B^{[4]}$ units in the glass by replacing some of the $B^{[4]}$ sites with $Al^{[4]}$ sites[38, 39]. The structure of Al and B in aluminoborates is also dependent on the concentration and type of modifiers. Just as for their silicate counterparts, Al has been found to exist in higher coordinated Al speciation, i.e. $Al^{[5]}$ and $Al^{[6]}$. These higher coordinations of Al with oxygen tend to occur in cases where the ratio of modifiers to Al_2O_3 is less than 1 and in cases where modifiers with high field strength cations are used[38, 39]. Aluminoborate glass structures are complex structures that can show the presence of various structural units: $B^{[3]}$, $B^{[4]}$, $Al^{[4]}$, $Al^{[5]}$, $Al^{[6]}$ units with varying coordination of NBOs (i.e.$^{[1]}$, $O^{[2]}$, $O^{[3]}$). Various interactions between the units can exist in the structures of these networks such as $B^{[3]}$+$Al^{[4]}$ or $B^{[4]}$+$Al^{[6]}$[37]. Structures with high field strength modifiers favor distributions like $B^{[4]}$+$Al^{[6]}$, $B^{[3]}$+$Al^{[5]}$ and $B^{[3]}$+$Al^{[6]}$[38, 45]. The degree of mixing of these network-forming species, Al and B, is a key consideration in the control of properties of these glasses such as chemical durability, viscosity, and strength, hardness and crack resistance[13, 46]. There still is not a complete model that details the relationships between structure and properties in aluminoborates[2], therefore more studies need to be conducted on the topic.

2.4 – Structure and hardness

The hardness of a material is defined as the resistance of material towards elastic and plastic deformation upon application of a load[47]. Hardness is a qualitative estimate of the strength of the intermolecular bonds in a material[48]. The hardness of a glasses is usually determined by an indentation method i.e. Vickers, Knoop, etc[2, 47]. During the indentation process, an indenter with a tip made of a hard material (typically diamond) is loaded onto the surface of the glass with a load applied to it. The tip leaves an impression on the glass once the load is removed. The dimensions of this impression are used along with the value of the load applied to determine the hardness of the glass[2, 47].

As previously stated, Al_2O_3-rich glasses have shown good mechanical properties in terms of hardness (see Figure 1), which could be attributed to the high bond dissociation energy of Al–O bonds (512±4 kJ/mol.)[15]. This affects its resistance to deformation. Al_2O_3-rich aluminosilicate glasses with the hardness values (8 – 9.5 GPa) recorded have significant amounts of alumina in their compositions[48-50]. The initial studies pertaining to aluminosilicate glasses contain up to 30 mol.% of Al_2O_3 in the system of Al_2O_3-Y_2O_3-SiO_2 with added TiO_2 and La_2O_3 by Makishima et al[49]. The observed mechanical behavior were explained in terms of the dissociation energies of the constituent oxides and their atomic packing factors in the glasses since oxides with higher dissociation energies and atomic packing factors displayed higher elastic modulus[49]. Further, a study by Johnson et al.[50] observed a positive correlation between the mechanical properties (hardness and Young's modulus) of a RE_2O_3-Al_2O_3-SiO_2 (RE_2O_3 = Y_2O_3, La_2O_3, ErO_2, YbO_2) series and Al_2O_3 content.

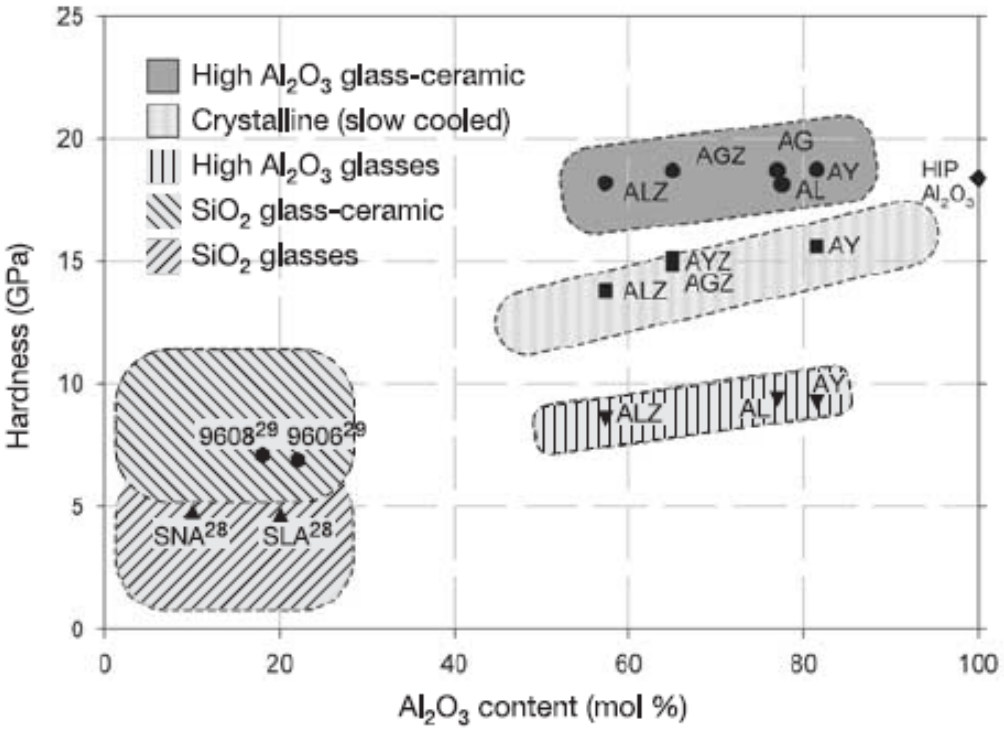

Figure 1: Hardness versus Al_2O_3 content for various classes of materials. Figure is copied from Rosenflanz et al.[10]

In addition to bond dissociation energy, an increase in $Al^{[5]}$ and $Al^{[6]}$ is accompanied by an increase in the hardness of these glasses due to an increase in packing and rigidity of the network[4, 48]. For example, studies done by Rosales-Sosa et al. showed that with an increase in coordination in Al, an increase in hardness and moduli was observed[4]. The authors attributed the high hardness to the high dissociation energy per unit volume of the Al_2O_3 bonds. Similarly, the high hardness in a series of RE_2O_3-Al_2O_3-SiO_2 (RE = Y, La, Lu, Sc) glasses was attributed to an increase in the coordination number of Al[48]. Other studies have also correlated high mechanical properties in glasses with high packing density of the glasses as well as unusual preeminence of higher coordination of the aluminum cation in their structures[14, 51, 52].

Recently, studies on structural and mechanical properties of aluminoborate glasses have consistently shown similar behavior of hardness increase with increase in Al coordination number [11, 42, 53, 54]. In addition to it, hardness has been shown to increase with an increase in $B^{[4]}$ units in these systems, as a result of the higher packing density in these systems[11, 13, 42]. Previous studies on several alkali and alkaline-earth aluminoborate glasses and their subsequent high-pressure densification have shown an increase in Al and B coordination upon densification[42, 55, 56]. Upon hot compression, the coordination number of both Al and B increases from $Al^{[4]}$ to $Al^{[5]}$ and $Al^{[6]}$ and from $B^{[3]}$ to $B^{[4]}$[11, 42]. Furthermore, similar to aluminosilicate glasses, the increase in hardness is positively correlated to the increase in the packing density upon densification[4, 48-51].

Understanding of the role of network modifiers is also important in addition to understanding the structure of network formers in a glass. Modifier cations with high field strength tend to play an important role in Al-containing glasses by increasing the average coordination of Al[39, 48, 52]. The field strength of a cation is the ratio of the charge of the cation to its radius according to Dietzel[57]. Rare-earths along with scandium, yttrium, divalent cations (especially magnesium and calcium) as well as several of the transition metal ions are generally considered to be high field strength cations. In conjunction with high alumina content, rare-earth oxides have often been used in various compositions for high hardness[10, 48-51] where they have shown interesting mechanical properties. Additionally, choice of the high field strength cation is important as well. Previous studies have shown that glasses with rare-earth oxides with higher ionic radii displayed better glass-forming ability, although lower hardness, than those glasses with rare-earth oxides with smaller radii[10, 50, 58].

2.5 – Structure and crack resistance

Despite high hardness, glasses suffer from brittleness. Glasses, especially oxide glasses, do not possess proficient plastic bulk dissipation mechanisms of energy[59] i.e. they experience little macroscopic plastic deformation before failure. This lack of stress and energy dissipation mechanisms contributes to their brittleness. A parameter, crack resistance can be used to assess resistance to radial cracking in a glass[60]. Radial cracks emanating from indentations vary with various loads, with the number of cracks increasing with increasing loads[60]. Crack resistance is defined as the load where the probability of cracking with radial cracks is 50%, or the load where the average of radial cracks of an indent is 2 out of a maximum of 4 after indentation[60]. Further, previous studies have associated crack resistance of a glass with the stress induced deformation mechanisms[61, 62].

There are various deformation mechanisms a glass can be subjected to during indentation as shown in Figure 2. Densification is one of two permanent deformation mechanisms that can occur in a glass, the other being shear flow[61, 63]. Densification is a non-volume conservative plastic deformation mechanism that tends to occur in materials with low atomic packing density[61]. The second mechanism, shear flow, is a volume conservative plastic deformation mechanism that takes place after the material can no longer densify, as it has a higher energy threshold associated with it[61]. Furthermore, the indentation deformation mechanism in glasses has been correlated to the Poisson's ratio (ν) of glasses. Glasses with low Poisson's ratio have open structures. As a result, they tend to deform by the densification mechanism[61, 63], whereas, glasses higher Poisson's

ratio, tend to deform through a shearing mechanism as their networks are more compact, i.e. metallic glasses[61, 63]. Oxide glasses generally, tend to have low Poisson's ratio ($\nu < 0.3$)[63]. Thus, these would be mostly associated with the densification mechanism.

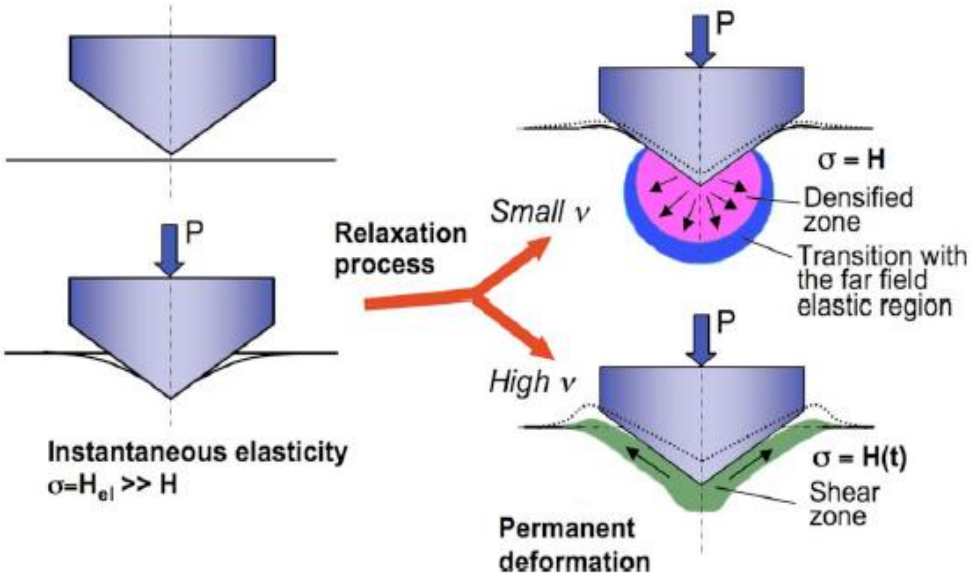

Figure 2: Different deformation mechanisms that can take place in a glass. Figure copied from original work[61].

Early studies into improving intrinsic properties of brittle materials includes a study by Sehgal et al[64]. The authors investigated a series of soda-lime-silica (SLS) glasses and found that the brittleness of the glasses is influenced by the atomic packing density of glasses i.e. glasses with higher molar volume, therefore more open structures were found to have lower brittleness. These authors subsequently developed a low-brittleness SLS glass which had a crack initiation load 10 times higher than that of commercial SLS, but with a lower hardness value and Young's modulus when tested in N_2 atmosphere. Subsequent studies were successful in designing and synthesizing oxide glasses in various families with high crack initiation loads, but the hardness values were considered

low (5-6 GPa)[65-68]. Studies on an alkali-free aluminoborosilicate series and a soda borosilicate series have shown that crack resistance varies with boron speciation in the structure[66]. A recent study by Limbach et al[67] correlated the crack resistance to the composition in a series of borosilicate. However, no direct correlation was found between the hardness and crack resistance of any of these glasses although composition and structure seemed to have an influence on their hardness and crack resistance.

Previous studies on aluminosilicate glasses highlight the fact that a high packing density and high bond dissociation energies of the constituent oxides in the glasses is positively correlated to the hardness[4, 14, 48-51]. Furthermore, high crack resistance has been mostly associated with densification in glasses under sharp contact loading [64-67]. As a result, high crack resistance has been generally found to be mutually exclusive with high hardness in glasses. However, recently, Rosales-Sosa et al. fabricated a series of glasses that displayed both high hardness and crack resistance[4]. The series of xAl_2O_3-(100-x)SiO_2 (x = 30-60 mol.%) glasses displayed increasing packing density, Poisson's ratio, hardness, and crack resistance with increasing Al_2O_3 content. In this study, crack resistance of the glasses increases with increase in the atomic packing density. This study not only reaffirmed the apparent dependence of hardness and crack resistance on composition and structure, but it also demonstrated that it is possible to have both high hardness and high crack resistance in oxide glasses.

Recent studies have shown promising results in aluminoborate glasses in terms of crack resistance and hardness. A recent study published by Januchta et al[11] reported on the disco of a bulk oxide glass of composition 24 Li_2O – 21 Al_2O_3 – 55 B_2O_3 (mol.%), with one of the crack resistance values observed (30 N). The authors attributed the

record-high crack resistance value to the ability of the glass to self-adapt under stress, with the network-forming cations, Al and B, changing their coordination in order to dissipate the elastic energy. In studies of their counterparts where the modifier was Na instead of Li, the glasses with Li showed consistently higher hardness values, affirming that the type of modifiers content also play a role on the structure of Al and B in aluminoborates. In another one of the work published by the same group, the hardness decreased with substitution of larger alkali modifiers from 4.1 GPa for the glass with Li_2O to 2.0 GPa for the glass with Cs_2O[43]. This was shown to be due to different causes such as atomic bonding energy and packing efficiency in the networks in addition to the ability of the network to self-adapt. Although some more work has been published regarding different composition-structure-property of aluminoborates[43, 44], there is still some work needed to understand in more details how these systems work.

Chapter 3 – Experimental Approach

3.1 – Design

From the literature review above, Al_2O_3–rich aluminoborate glasses present themselves as potential candidates for advanced application which require high hardness and crack resistance. High contents of Al_2O_3, especially in 5-coordination, have a positive correlation with hardness[4, 10, 11, 13, 14, 42, 48-51, 53, 54] while this generally has an adverse impact on the crack resistance of these glasses[64-68], making the glasses more brittle. Incorporation of B_2O_3 in the glass can increase crack resistance as $B^{[3]}$ units in the borate glass structure promote densification under sharp contact loading[11, 13, 42-44, 55]. The glass dissipates these stresses by undergoing structural changes and decreasing the free volume. Therefore, it is possible to design compositions to yield favorable structural units with high stress absorption abilities.

According to the above-mentioned perspective, two main characteristics that were considered to design compositions exhibiting high hardness and crack resistance were high alumina content and high $B^{[3]}/B^{[4]}$ ratio. Further considerations were given to network modifying cation in the glass system. As previously covered, rare-earth oxides in glasses have been shown to yield high hardness[10, 48-51]. In the case of rare-earth oxide, special attention must be paid when using them as these oxides are on the heavy sides of oxides with high densities. Substantial concentrations of rare-earth oxides in glass compositions positively scale with high densities[50]. Furthermore, oxides with larger ionic radii, therefore higher densities, display larger glass formation ability[10, 50].

As part of a literature survey for aluminoborate glass compositions that have been shown to have good mechanical properties, a commercial glass property database,

SciGlass, was used. Consequently, we found a study that had been conducted before looked at several properties of a series of yttrium aluminoborates[54]. The glass formation diagram for that study is shown in Figure 3.

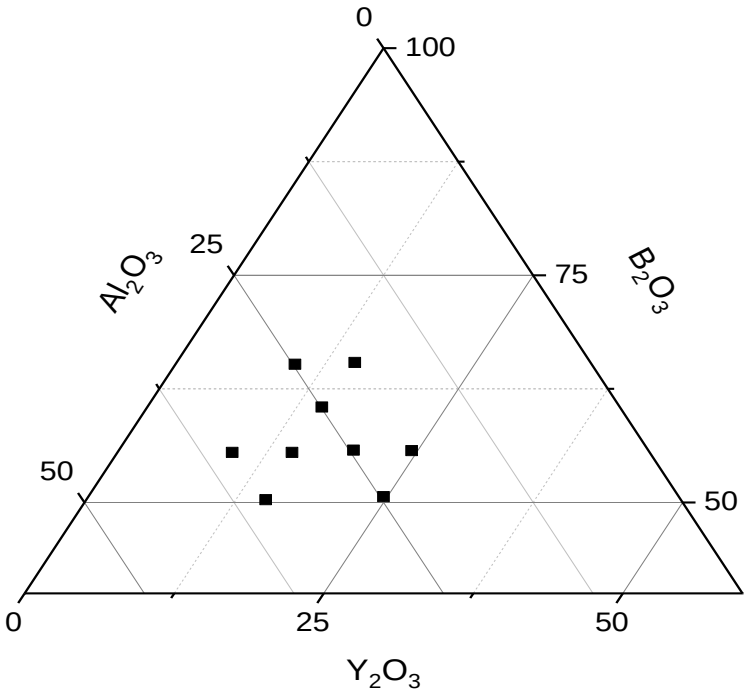

Figure 3: Diagram of Y_2O_3-Al_2O_3-B_2O_3 series compositions synthesized by Rutz et al.[54] as reproduced from original work.

One of the glasses in that series with high alumina content and high hardness values was chosen as the starting point for this study with the composition of 9.6 Y_2O_3 – 34.9 Al_2O_3 – 55.5 B_2O_3 (mol.%). In our experiments, when melted, the melt devitrified upon cooling. Magnesium oxide was used to stabilize the composition with the rationale that due to its high field strength, it would polymerize the network by pulling the oxygen atoms to itself and would increase vitrification. Several compositions of the same family as well as a lanthanum aluminoborate family with high alumina content were synthesized at temperatures below 1650°C. Only studies regarding the magnesium yttrium

aluminoborate glasses will be presented in the following chapters. The compositions investigated are presented in Table 1.

Table 1: Compositions investigated in present study with values in mol.% Glasses are designated by their Al_2O_3 content.

Glass	**MgO**	**Y_2O_3**	**Al_2O_3**	**B_2O_3**
Al-30	x	y	30	100 – x – y - 30
Al-35	x	y	35	100 – x – y - 35
Al-40	x	y	40	100 – x – y - 40

3.2 – Synthesis

Powders of high purity were used to synthesize these glasses. Batches of Al_2O_3 (99% extra pure, Acros Organics), H_3BO_3 (99+% extra pure, Acros Organics), Y_2O_3 (99.9%, Alfa Aesar) and $(MgCO_3)_4{\cdot}Mg(OH)_2{\cdot}5H_2O$ (98%, Alfa Aesar) were well-mixed according to their respective compositions before being melted in Pt-10%Rh crucibles at temperatures ranging from 1600°C to 1650°C for 2 hours in an electric furnace. Dehydration and calcination steps were taken before the melting in order to dehydrate and calcine the precursors for boron trioxide and magnesium oxide. The glasses were made in batches of 70 g for characterization. After melting, the glasses were annealed at 700°C for 1.5 hours to remove residual internal stresses introduced during its quenching. Once annealed, the glasses were cut and processed for subsequent indentation. Glass pieces for the other characterization techniques (MAS-NMR and DSC) were obtained from splat-quenched glasses. A picture of the glass designated Al-35 is displayed in Figure 4. An x-ray diffractometer (PANalytical – X'Pert PRO, Cu Kα radiation with a

scan range from 10° to 90° and a scan step size of 0.01°/s) was used to verify that the samples of the series were amorphous.

Figure 4: Monolithic piece of Al-35 (MgO-Y_2O_3-Al_2O_3-B_2O_3) as-synthesized after annealing.

3.3 – Characterization

3.3.1 – Differential scanning calorimetry

A differential scanning calorimeter or DSC (Netzsch STA 449F5) was used to record and analyze thermal changes that take place in the samples. The samples were crushed to sizes ranging from 850µm to 1mm and heated up at various rates inside of Pt crucibles in N_2 atmosphere from 60°C to 1300°C. In the DSC system, two empty pans are used for a baseline calibration in order to establish a defined heat capacity over the range of temperatures the measurement are to be conducted for. After the baseline calibration is completed, material is added to one of the pans (sample pan) while the first pan stays empty (reference pan). Both pans then go through the same heating cycle. The amount of heat required to increase the temperature is recorded for both reference and sample pans.

The difference between the reference pan and the sample pan can be plotted as a function of temperature to determine the thermal changes that take place in the sample upon heating. The glass transition temperature (T_g), onset of crystallization temperature (T_c), peak of crystallization (T_p) and melting temperature (T_m) were all determined for the glasses. The thermal stability of the glasses was evaluated, and their activation energies calculated.

3.3.2 – Magic angle spinning – nuclear magnetic resonance

The structural characterization of the glasses was done using magic angle spinning - nuclear magnetic resonance (MAS - NMR). ^{11}B and ^{27}Al MAS-NMR was conducted for all the samples. Powders for the glasses were packed into 3.2 mm zirconia rotors with spinning of 15 kHz. The ^{11}B NMR and ^{27}Al NMR measurements were taken using a Varian 240-MR DD2 spectrometer, operating at a field of 5.6T and a 3.2 mm triple resonance MAS NMR probe. The ^{11}B NMR spectra were collected at resonance frequencies of 77.77 kHz using $\pi/6$-pulse durations, a delay of 0.55μs, a recycle delay of 0.1s. The ^{27}Al measurements were made on the same spectrometer operating at the same field. These spectra were collected at resonance frequencies of 63.16 kHz, using $\pi/6$-pulse durations, using a delay of 0.50μs, a recycle delay of 1s. Chemical shifts of ^{27}Al are reported relative to solid AlF_3 (measured at -16.05 ppm relative to a 1M aqueous solution of $Al(NO_3)_3$) and ^{11}B chemical shifts are reported relative to solid BPO_4 (measured at -3.5 ppm relative to $BF_3O(C_2H_5)_2$). Fittings were done using Gaussian/Lorentzian and Q MAS ½ functions from the software DMfit for ^{11}B NMR spectra. The CzSimple model

was used for the ^{27}Al NMR spectra using the same software. Speciation and abundance of both boron and aluminum in the glass structure were determined.

3.3.3 – Vickers indentation

The hardness (H_v) of the glasses was investigated using a Vickers indenter (Leco LM248AT). In the Vickers indenter, loads are applied to the sample with a pyramid shaped diamond tip with angles of 136°. The tip leaves an impression in the glass, whose dimensions along with the load applied, are used to quantify the hardness. The hardness of a sample using Vickers indentation is quantified using the formula in Equation (1)

$$H_v = 1.8544 \frac{P}{d^2} \quad (1)$$

where P is the applied load and d is the average of the two diagonals of the indents in units of N and mm^2 respectively. A glass sample of approximately 1.5cm by 1.5cm was cut, ground and polished to a surface roughness of approximately 3 µm. Acetone was used as a medium agent during the polishing process in order to prevent reactions between the surface of the glass and air as boron is extremely moisture sensitive. Indentation was performed on that glass in ambient conditions. Hardness values are reported for the glasses at a load of 200gf. A minimum of 20 indents and a dwell time of 10s are used for these indents.

3.3.4 – Crack resistance

The sample was indented at loads of 100, 200, 500, 1000, 2000 gf. with a minimum of 10 indents at each load for the glasses. The crack resistance of the glasses was determined from the microindentation data. By taking the number of corner cracks per indent and dividing by the total number of corners, the probability of the glass

cracking goes from 0% (no corner cracks) to 100% (all corners cracked) as the loads applied are increasing. The crack resistance of the glass is the load at which the probability of cracking is 50%.

3.3.5 – Density

The density (ρ) of the glasses was measured using Archimedes' principles. D-limonene, with a density of 0.841 g/cm^3 was used as the suspending fluid in ambient conditions. Measurements were made on a minimum of four different glass pieces, and the densities were averaged. The dry and submerged masses were measured with a balance accurate to the third decimal point. Using the density and NMR data, the atomic packing density (C_g) of these glasses was estimated. C_g is a ratio between the lowest volume occupied by the atoms of the glass and its molar volume. For this calculation, the constituent atoms of the network are assumed to be spherical with known ionic radii[69]. Coordination numbers for Al and B are taken from NMR results while octahedral coordination is assumed for Mg and Y atoms for simplicity. Cg is calculated according to Equation (2) where f is the molar fraction, N is Avogadro's number, A_xB_y is the chemical formula of the constituent, r_A and r_B are the ionic radii and M the molecular mass.

$$C_g = \frac{\rho \sum f_i [\frac{4}{3}\pi N(x r_A^3 + y r_B^3)]}{\sum f_i M_i} \quad (2)$$

The values used for the ionic radii are as followed for 0.72Å, 0.90 Å, 0.39 Å, 0.48 Å, 0.54 Å, 0.01 Å, and 0.11 Å for Mg, Y, Al$^{[4]}$, Al$^{[5]}$, Al$^{[6]}$, B$^{[3]}$ and B$^{[4]}$ respectively.

3.3.6 – Inductively couple plasma – mass spectroscopy

Inductively coupled plasma - mass spectroscopy was done on Al-35 to determine its elemental compositions. The difference between batched compositions and experimental compositions from ICP-MS results are shown in Table 2. The experimental compositions agree with the batched compositions. The difference between theoretical and experimental is less than 1 mol.% for each component for either glass. Boron is moisture sensitive and tends to volatilize easily at high temperatures[70-73]. The Al-35 glass had been melted twice at two different batch free times: one that had been re-melted for approximately 3 hours and the other one for 2 hours. Compositional analysis was done on the glasses to verify whether 1) the composition had retained its integrity through melting and 2) the batch free time had had any effect on the composition that had been batched. There does not appear to be any significant batch deviation from the batch composition in the glass.

Table 2: Difference in mol. % between experimental and batched compositions as determined by ICP-MS for two batches synthesized slightly differently: one batch melted for 2 hours and one batch re-melted for approximately 3 hours.

Element	**2 h**	**3 h**
Al_2O_3	0.24	0.14
B_2O_3	0.15	0.45
MgO	0.00	0.05
Y_2O_3	0.33	0.33

4 – Results and discussion

4.1 – Glass formation

The amorphous nature of the glasses was determined by X-ray diffraction (XRD) analysis (Figure 5). Al-30 and Al-35 exhibit good glass forming ability, whereas faster cooling rates (using splat quenching) are required for Al-40 to avoid crystallization. It had been previously mentioned that aluminates and glasses with high alumina content require high cooling rates, in the order of 10^3K/s or higher so that crystallization can be avoided[10, 21]. Further, critical cooling rate required for glass formation increases with increase in Al_2O_3/B_2O_3 ratio such that even splat-quenching is not adequate to avoid higher Al_2O_3-containing glasses from devitrifying.

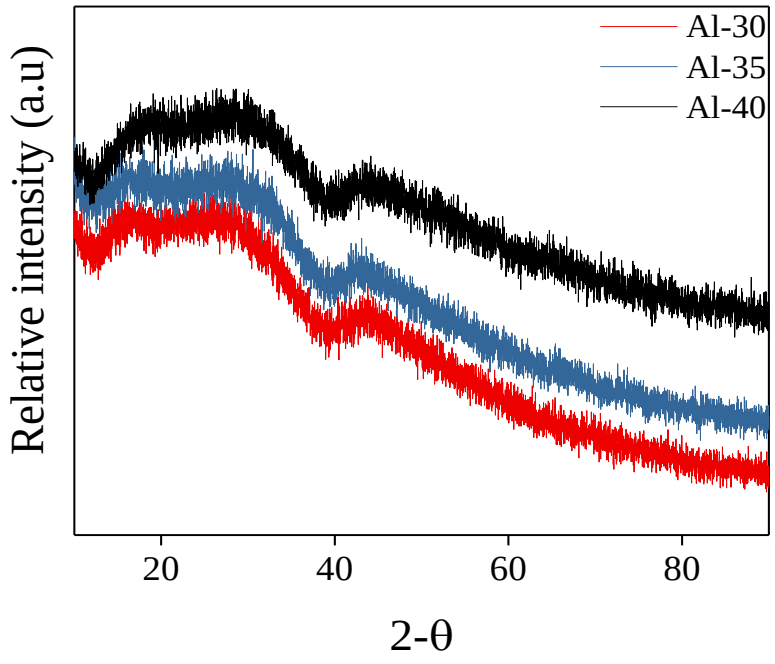

Figure 5: XRD of glasses, showing amorphous behavior. Only broad features can be observed on the spectra.

4.2 – Thermal parameters and stability

The thermal parameters for the glasses as determined by DSC measurements are presented in Table 3 for a rate of 30°C /min while the DSC graphs are shown in Figure 6.

Table 3: Thermal parameters (glass transition temperature (T_g), onset of crystallization (T_c), crystallization temperature (T_p), and melting temperature (T_m) as determined by DSC measurements for a rate of 30°C /min in N_2 atmosphere.

Glass ID	**T_g (°C)**	**T_c (°C)**	**T_{p1} (°C)**	**T_{p2} (°C)**	**T_{m1} (°C)**	**T_{m2} (°C)**
Al-30	717	894	915	---	1171	1178
Al-35	732	875	886	971	1171	---
Al-40	740	874	880	912	1175	---

With increase in Al_2O_3/B_2O_3 ratio, the glass transition temperature, T_g, increases from 717°C to 740°C. This thermal event was then followed by an exothermic crystallization peak that tends to appear at gradually lower temperatures from 894°C for Al-30 to 875°C for Al-35, and to 874°C for Al-40 with increasing Al_2O_3 content. For Al-30, a single crystallization curve is observed whereas with increasing the Al_2O_3 content to 35 mol.% then 40 mol.% results two distinct crystallization curves. The two distinct crystallization curves observed in DSC curve of Al-35 and Al-40 point towards a sequential precipitation of two different crystalline phases. Further, we observe an endothermic melting curve on the thermal spectrum ~ 1170°C. The DSC curve of Al-30 consists of two small melting ~1171°C and 1178°C. For Al-35 and Al-40, the curve shows sharp peaks ~1171°C and 1175°C, respectively. While the changes in T_g and T_c with substitution of B_2O_3 with Al_2O_3 are monotonic in nature, T_m exhibits a non-monotonous behavior with increase in Al_2O_3 content. Similar trends for the thermal curves were also

found for all the other heating rates at which the measurements were conducted (10, 15, 20 °C/min).

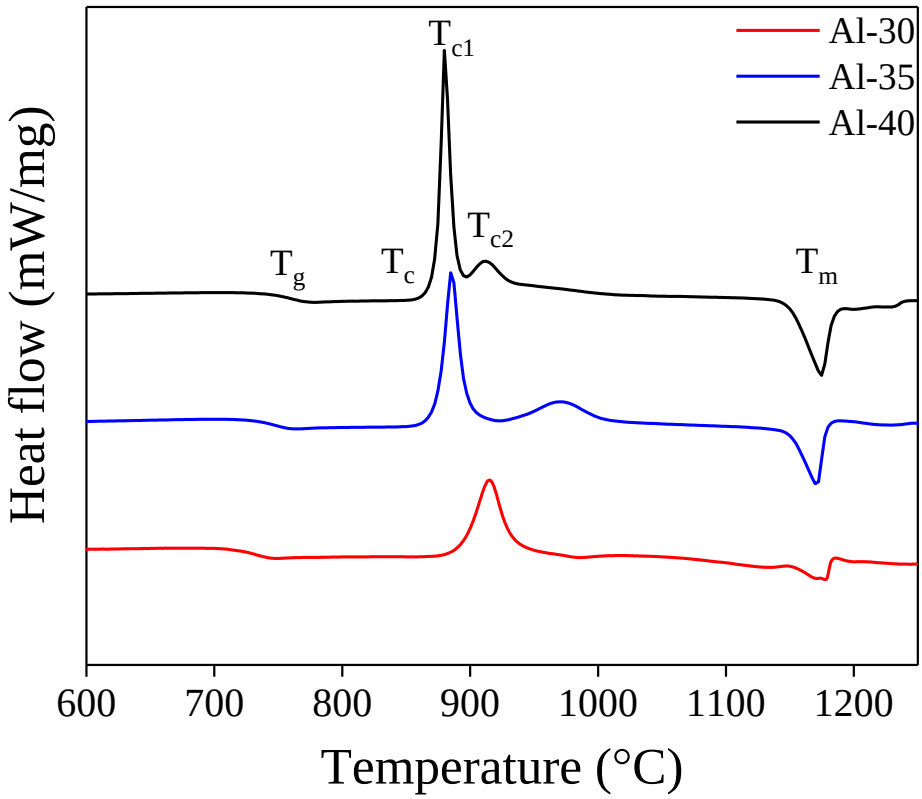

Figure 6: Curves of heat flow (mW/mg) versus temperature (°C) for series at a rate of 30°C/min in N_2 atmosphere.

The stability of the glasses against crystallization is calculated using the thermal stability parameter[72], ΔT (Table 4). The thermal stability refers to the difference between T_g and T_c ($\Delta T = T_c - T_g$). The greater the difference, higher is the glass stability towards crystallization [72, 73]. In the present investigation, ΔT decreases from 177°C for Al-30 to 134°C for Al-40 with increasing Al_2O_3 content in the series, indicating that glasses are more prone to crystallization with Al_2O_3 for B_2O_3 substitution.

The Hruby parameter (K_H) was also calculated for the glasses using Equation (3):

$$K_H = \frac{T_c - T_g}{T_m - T_c} \quad (3)$$

The Hruby parameter is a quantitative measure of how likely a glass will crystallize upon quenching and quantifies both the thermal stability and glass formation ability of a composition. The difference between T_c and T_g (ΔT) and the difference between T_m and T_c are directly and indirectly proportional to glass formation, respectively[74]. Higher values of the former indicate longer delays to nucleation while smaller values of the latter quantify shorter delays for growth[74-76]. A higher Hruby value indicates that the probability of crystallization of the glass is lower. The Hruby parameter for this series decreases with an increase in Al_2O_3 content, with a sharp decrease from Al-30 (0.64) to Al-35 (0.48) and a slower decrease to Al-40 (0.45) (Table 4). In agreement with the thermal stability parameter, the glasses become progressively more prone to crystallization with increase in Al_2O_3/B_2O_3 ratio.

Another parameter of quantifying the glass formation ability of glasses is the fragility index F. This parameter is used to measure the decrease of the relaxation time with temperature around the glass transition and is calculated according to the following equation:

$$F = \frac{E_\eta}{RT_g \ln 10} \quad (4)$$

Where E_η is the activation energy for viscous flow and R is the gas constant: 8.314J/mol.-K. Fragility ranges from kinetically strong glass-forming liquids with values of approximately 16 to kinetically fragile glass-forming liquids with higher values as high as 200[73]. The values for the investigated magnesium yttrium aluminoborate series ranging approximately from 37 and 60 (Table 4) and are higher than kinetically strong glasses

(~20). In coherence with the thermal stability and Hruby parameters, the fragility of the glasses increases with increase in Al_2O_3/B_2O_3 ratio. Furthermore, the increase in fragility from Al-35 to Al-40 is steeper than the increase in fragility from Al-30 to Al-35.

Further, we calculated the activation energy associated with the structural relaxation at the glass transition (E_{relax}), the activation energy for viscous flow (E_η) and the activation energies associated with the crystallization curves (E_c) where activation energies for the first (E_{c1}) and second crystallization (E_{c2}) curves (Table 4). The activation energies are calculated according to Equations (5) - (7):

$$\ln(\beta) = \frac{-E_{relax}}{RT_g} \tag{5}$$

$$\ln\left(\frac{T_g^2}{\beta}\right) = \frac{E_\eta}{RT_g} + \text{constant} \tag{6}$$

$$\ln\left(\frac{T_p^2}{\beta}\right) = \frac{E_c}{RT_p} + \text{constant} \tag{7}$$

where β is the rate at which the measurements are performed. The compositional scaling of activation energies follows a pattern similar to fragility where with the increase in Al_2O_3 content, the energies associated with transitions from one state to another, increases. The activation energies for structural relaxation around T_g (E_{relax}) and the activation energy for viscous flow (E_η) both increase with substitution of B_2O_3 for Al_2O_3 from 624 kJ/mol. to 1048 kJ/mol. and from 698 kJ/mol. to 1176 kJ/mol., respectively. The activation energies associated with crystallization (E_{c1} and E_{c2}) on the other hand, decrease from Al-30 to Al-40. E_{c1} decreases from 289kJ/mol. to 480 kJ/mol. while the E_{c2} values were 252kJ/mol. for Al-35 and 356kJ/mol. for Al-40.

Table 4: Stability indices (thermal stability (ΔT), Hruby parameter (K_H), fragility index (F) and activation energies associated with structural relaxation (E_{relax}), viscous flow (E_η), crystallization (E_c) for series.

Glass	K_H	ΔT (°C)	F	E_{relax} (kJ/mol.)	Eη (kJ/mol.)	E_{c1} (kJ/mol.)	E_{c2} (kJ/mol.)
Al-30	0.64	177	36.8	624	698	289	---
Al-35	0.48	143	55.0	943	1058	390	252
Al-40	0.45	134	60.7	1048	1176	480	356

The glass transition temperature increases with increase in Al_2O_3 content. The increase in T_g with the addition of Al_2O_3 is an effect of an increase in the Al coordination leading to an increase in the glass rigidity[77, 78]. Similar behavior has been observed in per-alkaline aluminoborate glasses[37, 38, 41, 45]. Further, the increase in fragility and crystallization tendency of the glasses agrees with literature, where an inverse correlation between glass stability and fragility has been observed for various oxide and metallic systems[79-81]. Along with the increase of fragility with increasing Al_2O_3, the activation energies associated with viscous flow and structural relaxation around the glass transition region increase. This stands to reason as the bond strength of Al_2O_3 (512 ± 4 kJ/mol.) is weaker than the bond strength of B_2O_3 (806 ± 5 kJ/mol.). Similarly, the activation energy of crystallization decreases with addition of Al_2O_3.

4.3 – Structural characterization

The ^{11}B NMR spectra for the glasses are shown in Figure 7 along with the deconvolution results from the DMfit software (Table 5). There are two distinctive features in these spectra. The network is comprised of both trigonal and tetrahedral units. First, there is a narrow peak located at 0 ppm. This peak is associated with the $B^{[4]}$ sites as it has been shown in other rare-earth aluminoborate glasses[38]. The first peak is overlaid on a broad asymmetric peak that ranges approximately from -37 ppm and 15 ppm. This peak is associated with the $B^{[3]}$ sites. The structure of the glasses consists of mostly trigonal boron units with only ~10% of the units being tetrahedral. The relative concentration of $B^{[4]}$ in the glasses ranges from approximately 12% in Al-30 to 8% in Al-40 (Table 5).

An increase in Al_2O_3/B_2O_3 ratio reduces the concentration of $B^{[4]}$ in the glasses. The plausible reason for this behavior is the stronger affinity of charge compensating cation towards the Al ion in comparison to the B ion[37, 38]. It has been shown before that modifiers tend to charge compensate Al ions before charge compensating B ions[38] due to the association of $Al^{[4]}$ to $B^{[3]}$ being more energetically favorable than the association of $Al^{[4]}$ to $B^{[4]}$[37, 44]. As a result, with the increase of Al_2O_3 content, a reduction in $B^{[4]}$ is observed in this series. Similar behavior has been observed in various other systems that include alkaline-earth and lanthanum aluminoborate systems[28, 37, 38].

The spectra for the ^{27}Al NMR are shown in Figure 8. The spectra of the investigated glasses consist of three peaks centered at ~60 ppm, ~30 ppm, and ~0 ppm with $Al^{[4]}$, $Al^{[5]}$ and $Al^{[6]}$ sites. respectively. Since, the glasses in the system are in the peraluminous region, 5-coordinated Al species are present in significant fraction ranging

between ~43% and ~46%. $Al^{[6]}$ has the minimum concentration in these glasses, with its concentration varying from ~19% in Al-30 to ~21% in Al-40 (Table 5). The addition of Al_2O_3 results in an increase in average coordination number of Al. This increase in coordination number is due to an increasing presence of Al and decreasing modifier for charge compensation.

Typically, with the addition of modifiers to binary alkali-borate glasses, T_g initially increases due to boron changing its coordination from 3 to 4 and the rigidity in the network increasing[2]. With the increase in $B^{[3]}$ and NBO with substitution of B_2O_3 for Al_2O_3 and increasing role of modifier of Al, a decrease in T_g is intuitive. In this case however, T_g still increases due to the rigidity of the network increasing and possibly Al_2O_3 having a higher melting temperature than B_2O_3. This connectivity increase is not due to boron, but aluminum. The effects of the structural changes in Al coordination overcome the effects of the structural changes in B in the glasses.

Table 5: Boron and aluminum fraction for different coordination for glass series. $B^{[3]}$ is mainly present while there are significant amounts of $Al^{[5]}$.

Glass	**$B^{[3]}$**	**$B^{[4]}$**	**$Al^{[4]}$**	**$Al^{[5]}$**	**$Al^{[6]}$**
Al-30	0.881	0.119	0.371	0.435	0.194
Al-35	0.893	0.107	0.361	0.441	0.199
Al-40	0.916	0.084	0.322	0.465	0.214

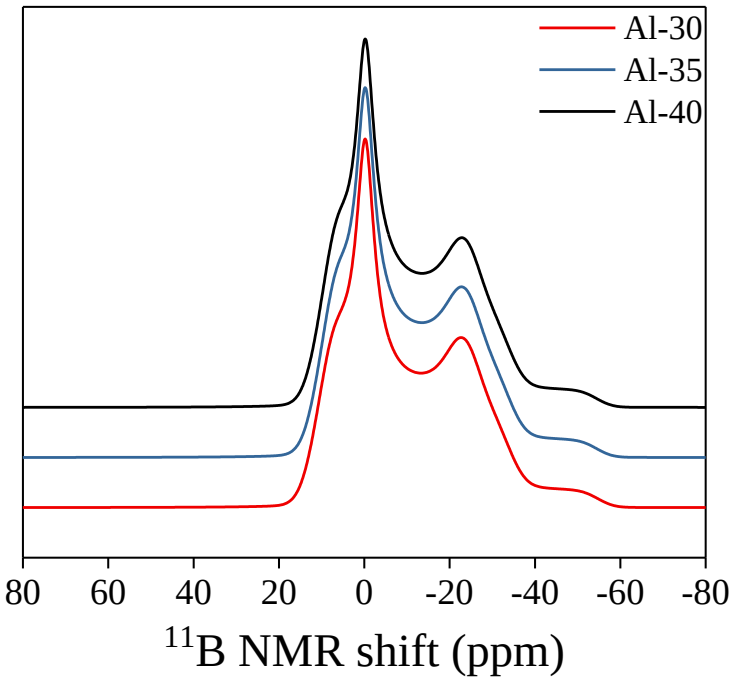

Figure 7: ^{11}B MAS NMR spectra for glasses.

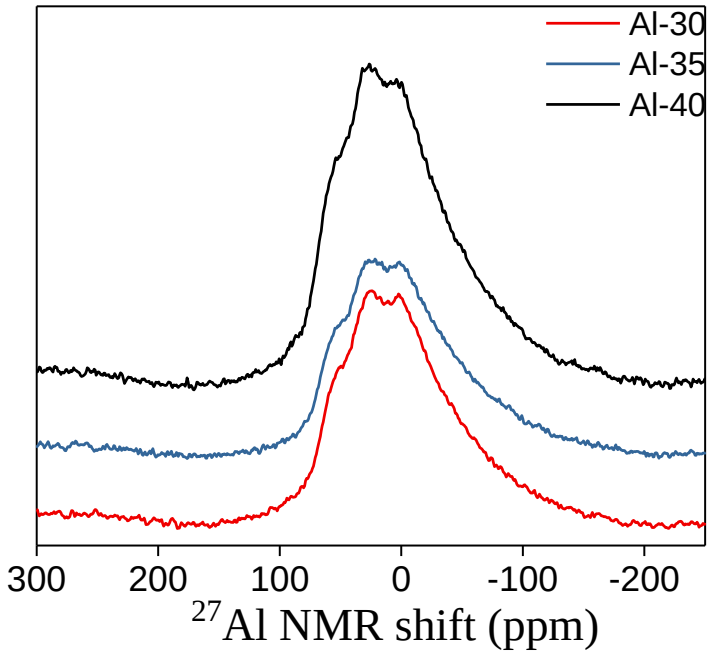

Figure 8: ^{27}Al MAS NMR spectra for glasses.

On the other hand, there is an increase in coordination of Al registered with increase of Al_2O_3/B_2O_3 ratio. The increase in coordination number in Al environment is due to an increasing presence of Al and decreasing modifier for charge compensation. In cases where Al is tetrahedral, it acts as a network former[28, 41]. Increasing the concentration of Al above a certain threshold, which depends on the modifying cation, causes Al to change its role from network former to network modifier[28]. With the increase of Al_2O_3 in this series, the fraction of $Al^{[4]}$ decreases while that of $Al^{[5]}$ and $Al^{[6]}$ increases, indicating a stronger modifying role for Al.

As mentioned earlier, MgO had been added in order to stabilize the composition and increase the glass stability in order to cast monolithic glass pieces. Mg^{2+} is a fairly small ion with a radius of 0.72Å according to Shannon[67]. Its field strength is subsequently $0.45Å^{-2}$. Y^{3+} is another high field strength cation ($0.57Å^{-2}$) whose oxide has a strong bond. Both of these high field strength cations are believed to promote hardness in the glasses, by promoting $Al^{[5]}$ formation (due to the cation attracting surrounding oxygen atoms). This is due to the fact that high field strength modifying cations can promote the stability of higher coordinated network forming cations[36, 37]. The networks then become more rigid and connected. This is reflected in the mechanical properties of the glasses. Similar effect of field strength on the Al speciation has been observed in previous studies[37, 38, 47, 50].

4.4 – Density and hardness

The density of the investigated increases with Al_2O_3 addition (Table 6). The increase in density could attributed to the density constituent oxides as the density of Al_2O_3 (3.98 g/cm^3) is higher than B_2O_3 (2.55 g/cm^3). In contrast with the density, the atomic packing density of the glasses decreases with the increasing Al_2O_3/B_2O_3 ratio. Due larger ionic radius of Al than B, packing is less efficient due to Al not fitting in the network as easily as B. Similar observations has been made in previous studies[37, 41].

Table 6: Glass transition temperature (T_g), density (ρ), atomic packing density (C_g), microhardness (H_v) and crack probability (%) at 2000 gf. for series.

Glass	**T_g (°C)**	**ρ (g/cm^3)**	**C_g**	**H_v (GPa)**	**Crack Probability (%)**
Al-30	717	2.97	0.646	7.26	15.5
Al-35	732	2.99	0.639	7.48	51
Al-40	740	3.05	0.633	7.81	52

The microindentation method reflects a relationship between the load to which the sample is subjected and the area of contact from the impression of the indenter used to deform the material as previously shown from Equation (1). The hardness of the glasses decreases with increasing loads attributed to the indentation size effect (see Figure 9)[82, 83]. The indentation size effect is a phenomenon observed in microindentation studies where an increase in hardness can be observed with decreasing penetration depth or decreasing loads for a given material and has been attributed to different factors such as elastic reco, work hardening, surface dislocation pining among other factors[82, 83].

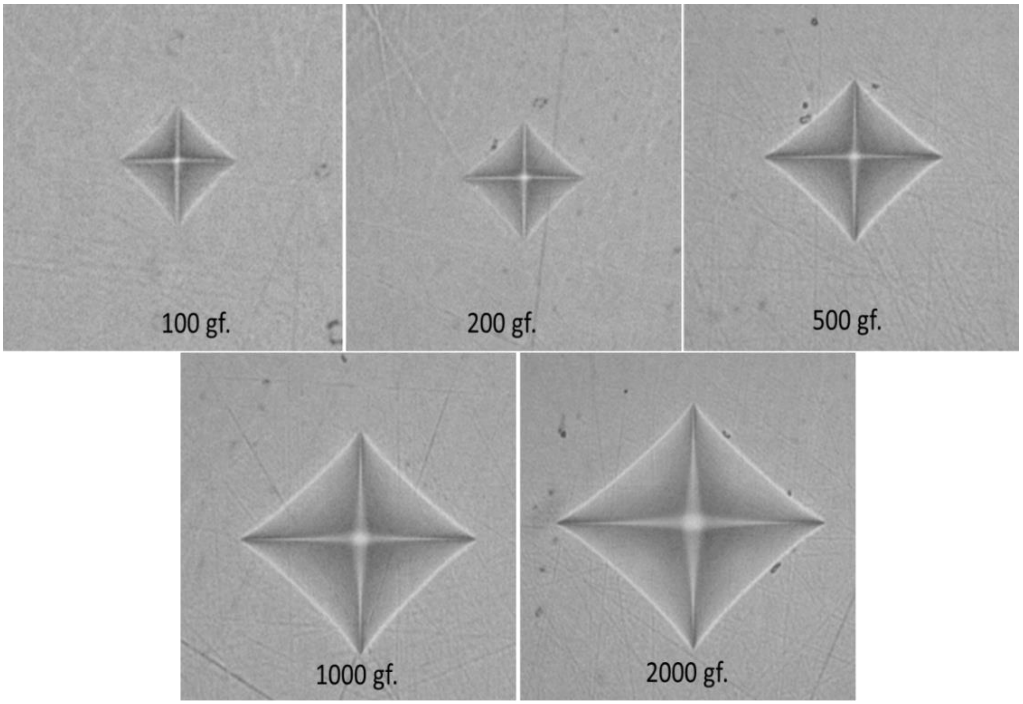

Figure 9: Microindentation of Al-35 at various loads ranging from 100 gf. to 2000 gf. Figure is not drawn to scale.

The hardness for the glasses increases from 7.26 GPa to 7.81 GPa with Al_2O_3 addition, with the hardness of Al-35 being 7.48 ± 0.029 GPa. It is noteworthy that, the H_V of the glasses at 200 gf. is on par or better for most commercial glasses that are currently available. For example, Corning's Gorilla glass has hardness of approximately 6.2 GPa, window glass has hardness of approximately 5.4 GPa while the hardness of Pyrex borosilicate is approximately 5.7 GPa [23-25]. The observed hardness of the glasses in this study is ascribed to the presence of high field strength cations with the significant fraction of high coordinated Al.

Mg^{2+} and Y^{3+}, as mentioned above, are both high field strength cations. Both of these cations have capable of highly polarizing the oxygen in their environments, attracting them closer, and leading to shorter and stronger bonds. As a result, the network

rigidity increases, thereby, increasing its resistance to elastoplastic deformation under sharp contact loading. This has been previously shown in different aluminosilicate and aluminoborate systems[10, 47-50]. The glasses in this series also show high amounts of higher coordinated Al. The increasing amounts of higher coordinated Al indicate increased connectivity which are shown in the NMR data. A positive relationship has been found with these previously mentioned different factors and the coordination number of Al^{3+}[47]. In terms of bond constraints, more bond constraints per atom has been shown to lead to a more rigid network, resulting in higher hardness[84, 85]. As there are more angular bond constraints per atom in glasses in $Al^{[5]}$ than in $Al^{[4]}$ and in $B^{[4]}$ than in $B^{[3]}$. More specifically, there are 3 of these constraints per $B^{[3]}$ and 5 per $B^{[4]}$ as well as 5, 7 and 9 per $Al^{[4]}$, $A^{[5]}$, and $Al^{[6]}$[85]. As a result, structures with higher coordination numbers present are more rigid, which causes them to have higher hardness values, as has been seen in glasses with increasing contents of $Al^{[5]}$ and $B^{[4]}$[11, 13, 41, 52, 53]. Similar behavior has been observed in several other studies where high fraction of higher coordinated aluminum was correlated with relative high hardness[4, 14, 47, 49].

Additional measurements were conducted for the elastic moduli and Poisson's ratio of Al-35. Young's modulus, shear modulus, bulk modulus was found to be 102 GPa, 39.6 GPa and 81.6 GPa (Table 7). The Poisson's ratio, ν, was found to be 0.29 GPa. Elastic moduli and Poisson's ratio for the other two glasses of the series, Al-30 and Al-40 are not expected to vary significantly from Al-35 based on the trends that were observed with the local structure of the glasses, their hardness and densities. The value of ν supports the efficient packing of the network. Poisson's ratio, which correlates with packing density in glasses, is relatively high, for these compositions. For oxide glasses, ν

is usually well below 0.3 for silicates and borosilicates while rare-earth aluminates and silicates are around 0.3[61, 86]. In this glass, ν = 0.29, which indicates a high atomic packing density, corroborated by the values calculated in Table 6.

4.5 – Crack resistance

A representative image of indents at various loads is shown in Figure 9. At 2000 gf., the probability of the glasses cracking was 15.5%, 51%, and 52% for Al-30, Al-35 and Al-40 respectively. The crack probability data was tentatively fitted using a sigmoidal function. While the fit for Al-30 was successful, the fits for AL-35 and Al-40 failed due to fewer data points. However, the crack probability for both of those glasses was slightly over 50% (51% and 52% respectively) at 2000 gf. Crack resistance for those glasses can be approximated to 2000 gf. for those glasses. The crack probability for the glasses as a function of Al_2O_3 content is shown in Figure 10 below. Crack resistance for Al-35 was subsequently found to be ~2075 gf. with a crack probability of ~15% at 2000 gf.

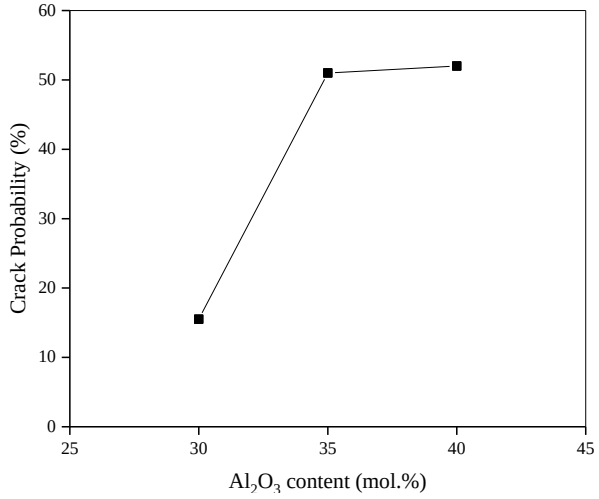

Figure 10: Crack probability versus Al_2O_3 content in glass at 2000 gf.

The crack resistance of these current glasses is relatively low when compared to other oxide glasses that were tested in ambient conditions. These other studies encompass silicate[64, 87], borosilicate[64, 65], and aluminoborate[11, 41] glasses. having crack resistance range from ~1200 gf. to ~3450 gf. and Vickers hardness values ranging from 3.2 to 5.7 GPa. Although the crack resistance for these glasses is lower here, their hardness is comparatively higher. In various other studies, crack resistance has been shown to decrease with increasing hardness in different systems[11, 14, 41, 64, 87]. In few cases, both hardness and crack resistance values has been shown to increase in a given series[4, 12]. Here, although the correlation between hardness and crack resistance is negative, both values are relatively high in comparison to past studies[11, 41, 64, 65, 87].

The crack resistance of this glass can be explained in terms of its structure. The investigated glasses exhibit significant presence of $B^{[3]}$ structural units. Almost 90% of the B_2O_3 is composed of $B^{[3]}$ species, which is more open than a $B^{[4]}$ prevalent network is, as corroborated by NMR results discussed earlier. The high amounts of $B^{[3]}$ is expected to accommodate dissipation of energy introduced by the indentation by changing its short-range structure, as this structure is more flexible than its $B^{[4]}$ counterpart[41, 64]. In borate-based glasses where high-pressure compaction was performed, it had been shown that the glass network was able to densify via local structural re-arrangement[12, 13, 41, 42].

Previous studies on crack resistance have shown a dependence on free volume in the network, where glasses with lower atomic packing density show higher crack resistance due to high degree of densification upon application of pressure[62-65]. Densification has been shown to enhance crack resistance more than shear flow as

densification results in lower residual stress, which reduces the driving force for cracking more than shear flow does[58]. Glasses with less rigid networks are typically more appropriate to promotion of densification. It has been shown that in aluminoborates, glasses with high amounts of $B^{[3]}$ show higher capabilities for densification[58, 64]. Although the extent of plastic deformation by densification is not investigated, the network structure of these glasses leads to believe that densification is the prominent deformation mechanism, which leads to a relatively high crack resistance as has been shown in different systems[11, 41].

Chapter 5 – Conclusions

In this work, an attempt was made to understand the drivers that govern the relationships between the composition, structure and properties of a relatively unexplored family of aluminoborate glasses with high alumina content (30 – 40 mol.%) using traditional melting methods, i.e. melt-quench. The system is comprised of MgO – Y_2O_3 – Al_2O_3 – B_2O_3. The compositional (using ICP-MS), structural (using MAS-NMR), mechanical (using Vickers indentation) and thermal (using DSC) behavior of a series of glasses that showed high hardness and relatively good crack resistance were investigated. A hardness of 7.48 GPa and crack resistance of ~2000 gf. were found for one of these glasses, with 35 mol.% of Al_2O_3. This aluminoborate glass was found to retain its composition at high temperatures for extended amounts of time and showed relative thermal stability based on the thermal stability (ΔT) and Hruby (K_H) parameters. The glasses display high $B^{[3]}$ (~90%) and $Al^{[5]}$ (~40%) contents, which are believed to promote hardness and crack resistance in these compositions. It is also possible to expand this system to include other rare-earth oxide modifiers. This study supports that it is possible to have glasses that have both good hardness and crack resistance, two properties that are usually mutually exclusive, by understanding the roles of different components in these glasses and tailoring compositions.

Chapter 6 – Limitations and Future Work

6.1 – Ballistics test

Big monolithic pieces of Al-35 have been prepared with the intention of testing for ballistic impact response (see Figure 11). The glass was scaled up to dimensions of 10 cm. by 10 cm. by 1.25 cm. using a graphite mold. The ballistic tests will look at properties of this glass and compare them to glasses that are currently used in current defense application to see how it behaves with respect to those other glasses.

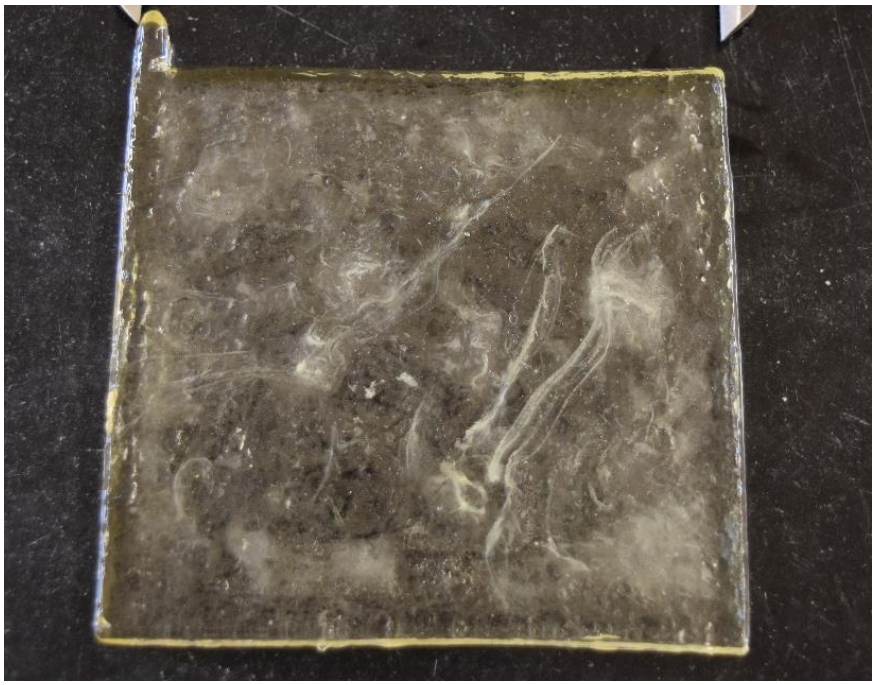

Figure 11: Scaled up piece of Al-35 glass for ballistics impact response tests. Inhomogeneities can be observed in the glass due to the small forming region in this glass family and scaling up the composition.

6.2 – Composition stabilization

When Al-35 was scaled up to centimeter scales pieces, not only it had to be quenched between two graphite plates to bypass minimal surface crystallization, inhomogeneities could also be observed in the slab (see Figure 11) as a result of the

composition being close to the glass formation boundaries and being prone to crystallization. It is necessary to increase the glass formation region of this composition by potentially adding small amounts of traditional glass-formers with the purpose of increasing the processability region of this composition.

6.3 – Physical properties and chemical durability studies

Several mechanical and optical properties of this glass have not been determined yet. Properties such as flexural and tensile strengths, fracture toughness, refractive index, and coefficient of thermal expansion have not been determined for this glass. These could be more useful into developing a more complete understanding of these glass systems. An additional property that would be beneficial to investigate is the dissolution rate of this glass. Because a high component of this glass is boron trioxide, the durability of the composition is extremely important. Borate glasses are notorious for their faster dissolution rates when compared to their silicate counterparts. Al-35 is also largely composed of alumina (35 mol.%). How exactly the glass will behave is not exactly known. Dissolution rate studies that had been conducted on the series of which the parent glass is of (Y_2O_3-Al_2O_3-B_2O_3) showed dissolution rate of 3.9 and 5.0 $\times 10^{-7}$g cm^2/min in pH 1 of HCl for glasses with approximately 35mol.% of Al_2O_3[54]. The addition of magnesium oxide is not expected to have any negative effect on its durability, but quantitatively, this must be determined through chemical durability studies.

6.4 – Further RE-aluminoborate compositions exploration

In addition to Al-35, a glass piece of La_2O_3 - $38Al_2O_3$ - B_2O_3 (mol.%), called LAB, was synthesized using a procedure like the one for Al-35. A monolithic piece was obtained with values of 6.7 GPa for microhardness at 200 gf. Its density was found to be 3.22 ± 0.008 g/cm^3. This glass did not show any cracks up to 1000 gf. The density of this glass is higher than the density of Al-35 (the molar mass of La_2O_3 is higher than Y_2O_3's). It appears that other rare-earth elements might be good candidates for such glasses and it is a route that might be worth exploring.

Chapter 7 – Supplementary results

7.1 – Plots for determination of activation energies

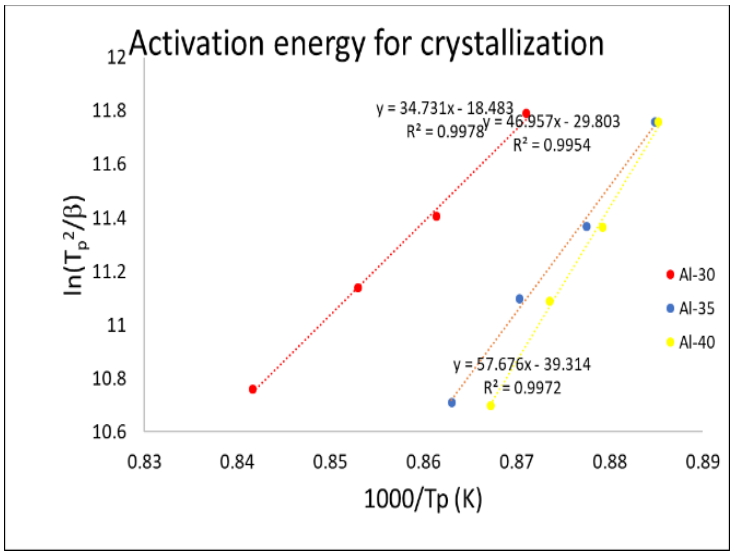

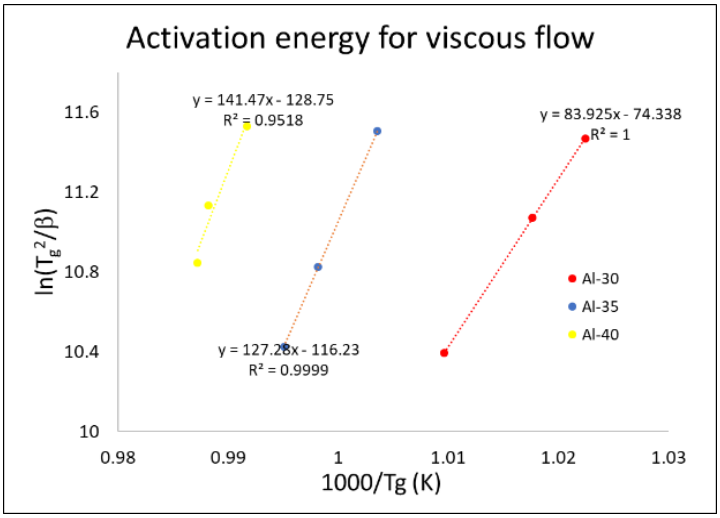

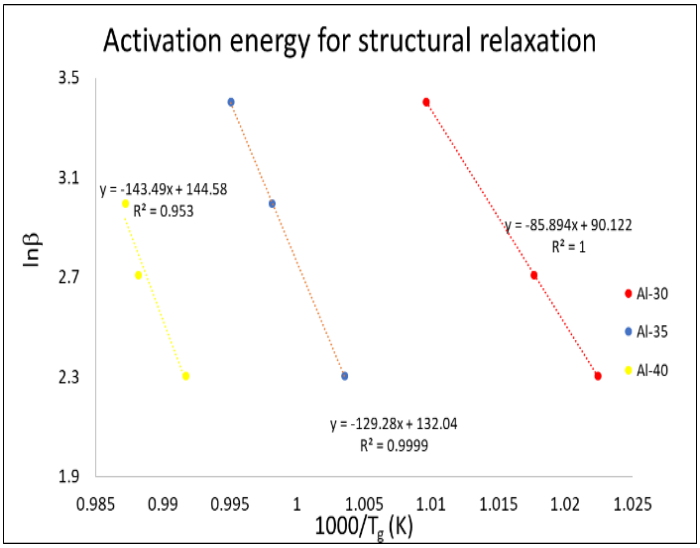

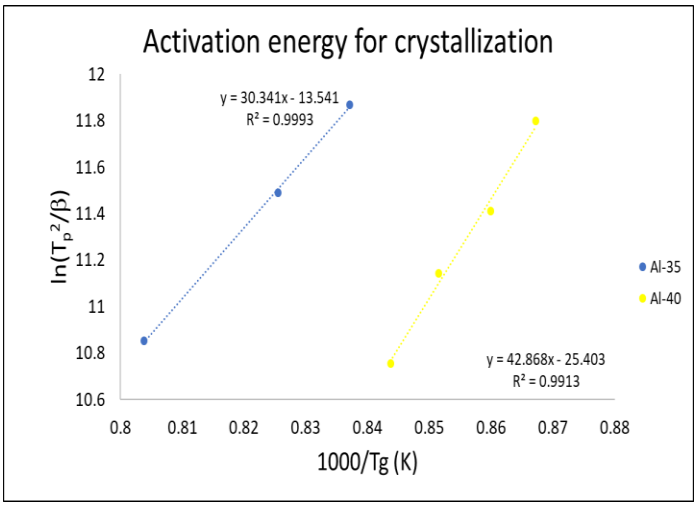

7.2 – Brillouin spectroscopy

The elastic properties were determined by Brillouin spectroscopy. The elastic moduli and Poisson's ratio were calculated from values determined experimentally from the density and both transverse and longitudinal Brillouin frequency shifts. The equations used to calculate the elastic moduli and Poisson's ratio are shown in Equations (8) - (11):

$$E = 2G\,(1 + \nu) \tag{8}$$

$$G = \rho V_T^2 \tag{9}$$

$$B = C_{11} - \frac{4}{3}G \tag{10}$$

$$\nu = \frac{3B - 2G}{6B + 2G} \tag{11}$$

In these equations E, G, B, and ν are respectively Young's modulus, the shear modulus, the bulk modulus, and Poisson's ratio. V_T is longitudinal and shear sound velocities while ρ represents the density of the glass. The values shown below are values for Al-35 glass in Table 7.

Table 7: Young's modulus (E), shear modulus (G), bulk modulus (B) and Poisson's ratio (ν) for Al-35.

Properties	**Values**	**Std. dev**
Young's modulus	102 GPa	0.6
Shear modulus	39.6 GPa	0.3
Bulk modulus	81.6 GPa	0.3
Poisson's ratio	0.291	0.001

References

1. Griffith, AA. The Phenomena of Rupture and Flow in Solids. Philosophical Transactions of the Royal Society of London Series A, Containing Papers of a Mathematical or Physical Character 1921;221:163-198.

2. Shelby, JE. Introduction to glass science and technology. Royal Society of Chemistry, 2005.

3. Gy, R. Ion exchange for glass strengthening. Materials Science and Engineering: B 2008;149(2):159-165.

4. Rosales-Sosa, GA, Masuno, A, Higo, Y, et al. Crack-resistant Al2O3-SiO2 glasses. Scientific Reports 2016;6.

5. Orowan, E. Notch, brittleness and the strength of metals. Glasgow: Institution of Engineers and Shipbuilders in Scotland, 1945.

6. Condon, EU. Physics of the Glassy State. I. Constitution and Structure. American Journal of Physics 1954;22(2):43-53.

7. Li, X, Lu, J, Feng, Z. Effect of hydrofluoric acid etching of glass on the performance of organic–inorganic glass laminates. Composites Part B: Engineering 2013;52:207-210.

8. Dériano, S, Rouxel, T, Malherbe, S, et al. Mechanical strength improvement of a soda-lime–silica glass by thermal treatment under flowing gas. Journal of the European Ceramic Society 2004;24(9):2803-2812.

9. Shim, G-I, Kim, C-Y, Choi, S. Strengthening of borosilicate glass by controlled crystallisation for lightweight bulletproof materials. 2013.

10. Rosenflanz, A, Frey, M, Endres, B, et al. Bulk glasses and ultrahard nanoceramics based on alumina and rare-earth oxides. Nature 2004;430(7001):761-764.

11. Januchta, K, Youngman, RE, Goel, A, et al. Disco of Ultra-Crack-Resistant Oxide Glasses with Adaptive Networks. Chemistry of Materials 2017;29(14):5865-5876.

12. Kapoor, S, Januchta, K, Youngman, RE, et al. Combining high hardness and crack resistance in mixed network glasses through high-temperature densification. Physical Review Materials 2018;2(6):063603.

13. Saurabh Kapoor, XG, Randall E. Youngman, Carrie L. Hogue, John C. Mauro, Sylwester J. Rzoska, Michal Bockowski, Lars R. Jensen, and Morten M. Smedskjaer. Network Glasses Under Pressure: Permanent Densification in Modifier-Free Al2O3−B2O3−P2O5−SiO2 Systems. Physical review applied 2017;7(5):054011

14. Rosales-Sosa, GA, Masuno, A, Higo, Y, et al. High Elastic Moduli of a 54Al2O3-46Ta2O5 Glass Fabricated via Containerless Processing. 2015;5:15233.

15. Dean, JA, Lange, NA. Handbook of chemistry. McGraw-Hill, 1999.

16. Oxide Ceramics - Aluminum Oxide (Al2O3): The Most Well-Known Oxide Ceramic Material; 2018. https://www.ceramtec.com/ceramic-materials/aluminum-oxide/. Accessed.

17. Jantzen, CM, Krepski, RP, Herman, H. Ultra-rapid quenching of laser-melted binary and unary oxides. Materials Research Bulletin 1980;15(9):1313-1326.

18. Weber, JKR, Abadie, JG, Hixson, AD, et al. Glass Formation and Polyamorphism in Rare-Earth Oxide–Aluminum Oxide Compositions. Journal of the American Ceramic Society 2004;83(8):1868-1872.

19. Foy, PR. Fabrication and characterization of calcium aluminate glass fibers. *Department of Materials Science and Engineering.* Ph.D. New Brunswick, NJ: Rutgers, The State University of New Jersey; 2008.

20. Prnova, A, Karell, R, Galusek, D. The preparation of binary Al2O3-Y2O3 glass microspheres by flame-synthesis from powder oxide precursors. Ceramics-Silikáty 2008;52(2):109-114.

21. Haliaková, A, Prnová, A, Klement, R, et al. Flame-spraying synthesis of aluminate glasses in the Al2O3–La2O3 system. Ceramics International 2012;38(7):5543-5549.

22. Prnova, A, Bodisova, K, Klement, R, et al. Preparation and characterization of Yb2O3-Al2O3 glasses by the Pechini sol gel method combined with flame synthesis. Ceramics International 2014;40(4):6179-6184.

23. Glass properties | Saint-Gobain; 2018. https://www.saint-gobain-sekurit.com/glossary/glass-properties. Accessed.

24. Corning Pyrex7740 Borosilicate Glass; 2018. Accessed.

25. Corning Gorilla Glass; 2018. https://web.archive.org/web/20140529230251/http://www.corning.com//docs//specialtymaterials//pisheets//PI2317.pdf. Accessed.

26. Schaeffer, HA. Scientific and technological challenges of industrial glass melting. Solid State Ionics 1998;105(1):265-270.

27. ASTM Compass; 2018. https://compass.astm.org/EDIT/html_annot.cgi?E3004+15e1. Accessed.

28. Sun, K-H. Fundamental condition of glass formation. Journal of the American Ceramic Society 1947;30(9):277-281.

29. Osipov, AA, Eremyashev, VE, Mazur, AS, et al. Coordination state of aluminum and boron in barium aluminoborate glass. Glass Physics and Chemistry 2016;42(3):230-237.

30. Dell, WJ, Bray, PJ, Xiao, SZ. 11B NMR studies and structural modeling of Na2O-B2O3-SiO2 glasses of high soda content. Journal of Non-Crystalline Solids 1983;58(1):1-16.

31. Sen, S, Xu, Z, Stebbins, JF. Temperature dependent structural changes in borate, borosilicate and boroaluminate liquids: high-resolution 11B, 29Si and 27Al NMR studies. Journal of Non-Crystalline Solids 1998;226(1–2):29-40.

32. Du, L-S, Stebbins, JF. Network connectivity in aluminoborosilicate glasses: A high-resolution 11B, 27Al and 17O NMR study. Journal of Non-Crystalline Solids 2005;351(43–45):3508-3520.

33. J. Kiczenski, T, Du, L-S, Stebbins, J. The Effect of Fictive Temperature on the Structure of E-Glass: A High Resolution, Multinuclear NMR Study. 2005.

34. Eigen, M. Chapter 12 - Oxide Glasses. In: Rao, KJ, ed. Structural Chemistry of Glasses. Oxford: Elsevier Science Ltd, 2002.

35. Mukhanov, VA, Kurakevich, OO, Solozhenko, VL. On the hardness of boron (III) oxide. Journal of Superhard Materials 2008;30(1):71-72.

36. Varshneya, A, K.,. Fundamentals of Inorganic Glasses, Second Edition. In: Society of Glass Technology, UK, 2013.

37. Bunker, BC, Kirkpatrick, RJ, Brow, RK. Local-structure of alkaline-earth boroaluminate crystals and glasses. 1. Crystal chemical concepts structural predictions and comparisons to known crystal structures. Journal of the American Ceramic Society 1991;74(6):1425-1429.

38. Bunker, BC, Kirkpatrick, RJ, Brow, RK, et al. Local-structure of alkaline-earth boroaluminate crystals and glasses. 1.B-11 and Al-27 MAS NMR spectroscopy of alkaline-boroaluminate glasses. Journal of the American Ceramic Society 1991;74(6):1430-1438.

39. Brow, RK, Tallant, DR, Turner, GL. Polyhedral arrangements in lanthanum aluminoborate classes. Journal of the American Ceramic Society 1997;80(5):1239-1244.

40. Brow, RK, Tallant, DR. Structural design of sealing glasses. Journal of Non-Crystalline Solids 1997;222:396-406.

41. Chan, JCC, Bertmer, M, Eckert, H. Site connectivities in amorphous materials studied by double-resonance NMR of quadrupolar nuclei: High-resolution B-11 <-> Al-27

spectroscopy of aluminoborate glasses. Journal of the American Chemical Society 1999;121(22):5238-5248.

42. Januchta, K, Youngman, RE, Goel, A, et al. Structural origin of high crack resistance in sodium aluminoborate glasses. Journal of Non-Crystalline Solids 2017;460:54-65.

43. Januchta, K, Bauchy, M, Youngman, RE, et al. Modifier field strength effects on densification behavior and mechanical properties of alkali aluminoborate glasses. Physical Review Materials 2017;1(6).

44. Frederiksen, KF, Januchta, K, Mascaraque, N, et al. Structural Compromise between High Hardness and Crack Resistance in Aluminoborate Glasses. Journal of Physical Chemistry B 2018;122(23):6287-6295.

45. Gresch, R, Müller-Warmuth, W, Dutz, H. 11B and 27Al NMR studies of glasses in the system Na2O · B2O3 · Al2O3 ("NABAL"). Journal of Non-Crystalline Solids 1976;21(1):31-40.

46. Du, L-S, Stebbins, JF. Site connectivities in sodium aluminoborate glasses: multinuclear and multiple quantum NMR results. Solid State Nuclear Magnetic Resonance 2005;27(1–2):37-49.

47. Varshneya, AK. Fundamentals of Inorganic Glasses. Elsevier Science, 2013.

48. Stevensson, B, Edén, M. Structural rationalization of the microhardness trends of rare-earth aluminosilicate glasses: Interplay between the RE3+ field-strength and the aluminum coordinations. Journal of Non-Crystalline Solids 2013;378:163-167.

49. Makishima, A, Tamura, Y, Sakaino, T. Elastic Moduli and Refractive Indices of Aluminosilicate Glasses Containing Y2O3, La2O3, and TiO2. Journal of the American Ceramic Society 1978;61(5-6):247-249.

50. Johnson, J, Weber, R, Grimsditch, M. Thermal and mechanical properties of rare earth aluminate and low-silica aluminosilicate optical glasses. Journal of Non-Crystalline Solids 2005;351(8-9):650-655.

51. Tanabe, S, Hirao, K, Soga, N. Elastic Properties and Molar Volume of Rare-Earth Aluminosilicate Glasses. Journal of the American Ceramic Society 1992;75(3):503-506.

52. Pahari, B, Iftekhar, S, Jaworski, A, et al. Composition-Property-Structure Correlations of Scandium Aluminosilicate Glasses Revealed by Multinuclear 45Sc, 27Al, and 29Si Solid-State NMR. Journal of the American Ceramic Society 2012;95(8):2545-2553.

53. Ghoneim, NA, El Batal, HA, M.A. Nassar, A. Microhardness and softening point of some alumino-borate glasses as flow dependent properties. Journal of Non-Crystalline Solids 1983;55(3):343-351.

54. Rutz, HL, Day, DE, Spencer, CF. Properties of Yttria-Aluminoborate Glasses. Journal of the American Ceramic Society 1990;73(6):1788-1790.

55. Bechgaard, TK, Goel, A, Youngman, RE, et al. Structure and mechanical properties of compressed sodium aluminosilicate glasses: Role of non-bridging oxygens. Journal of Non-Crystalline Solids 2016;441:49-57.

56. Svenson, MN, Bechgaard, TK, Fuglsang, SD, et al. Composition-structure–property relations of compressed borosilicate glasses. PHYSICAL REVIEW APPLIED 2014;2(2):024006.

57. Dietzel, A. Die Kationenfeldstärken und ihre Beziehungen zu Entglasungsvorgängen, zur Verbindungbildung und zu den Schmelzpunkten von Silicaten. Phys Chemie 1942;48:9-23.

58. Watanabe, Y, Masuno, A, Inoue, H. Glass formation of rare earth aluminates by containerless processing. Journal of Non-Crystalline Solids 2012;358(24):3563-3566.

59. Matteo, C. Stress-corrosion mechanisms in silicate glasses. Journal of Physics D: Applied Physics 2009;42(21):214006.

60. Kato, Y, Yamazaki, H, Yoshida, S, et al. Effect of densification on crack initiation under Vickers indentation test. Journal of Non-Crystalline Solids 2010;356(35-36):1768-1773.

61. Rouxel, T, Ji, H, Guin, JP, et al. Indentation deformation mechanism in glass: Densification versus shear flow. Journal of Applied Physics 2010;107:094903.

62. Sehgal, J, Ito, S. Brittleness of glass. Journal of Non-Crystalline Solids 1999;253:126-132.

63. Rouxel, T, Ji, H, Hammouda, T, et al. Poisson's Ratio and the Densification of Glass under High Pressure. Physical Review Letters 2008;100(22):225501.

64. Sehgal, J, Ito, S. A New Low-Brittleness Glass in the Soda-Lime-Silica Glass Family. Journal of the American Ceramic Society 1998;81(9):2485-2488.

65. M. Gross, T, Tomozawa, M, Koike, A. A glass with high crack initiation load: Role of fictive temperature-independent mechanical properties. 2009.

66. Kato, Y, Yamazaki, H, Kubo, Y, et al. Effect of B2O3 content on crack initiation under Vickers indentation test. Journal of the Ceramic Society of Japan 2010;118(1381):792-798.

67. Limbach, R, Winterstein-Beckmann, A, Dellith, J, et al. Plasticity, crack initiation and defect resistance in alkali-borosilicate glasses: From normal to anomalous behavior. Journal of Non-Crystalline Solids 2015;417-418(1-15):15-27.

68. Morozumi, H, Nakano, H, Yoshida, S, et al. Crack Initiation Tendency of Chemically Strengthened Glasses. International Journal of Applied Glass Science 2015;6(1):64-71.

69. Shannon, RDt. Revised effective ionic radii and systematic studies of interatomic distances in halides and chalcogenides. Acta Crystallographica Section A: Crystal Physics, Diffraction, Theoretical and General Crystallography 1976;32(5):751-767.

70. Cable, M. Kinetics of volatilization of sodium borate melts. Borate Glasses: Structure, Properties, Applications 1978:399-411.

71. Simon, JM, Smith, RA. Borate raw materials. Glass Technology 2000;41(6):169-173.

72. Grente, K, Rebillat, F, Langlais, F. Synthesis, characterization and high temperature corrosion of glass-ceramics in the B2O3-Al2O3-SiO2 system. *Electrochemical Society Proceedings Series.* 2003

73. Snyder, MJ, Mesko, MG, Shelby, JE. Volatilization of boron from E-glass melts. Journal of Non-Crystalline Solids 2006;352(6):669-673.

74. Goel, A, Shaaban, ER, Ribeiro, MJ, et al. Influence of NiO on the crystallization kinetics of near stoichiometric cordierite glasses nucleated with TiO2. Journal of Physics: Condensed Matter 2007;19(38):386231.

75. Goel, A, Shaaban, ER, Melo, FCL, et al. Non-isothermal crystallization kinetic studies on MgO-Al2O3-SiO2-TiO2 glass. Journal of Non-Crystalline Solids 2007;353(24-25):2383-2391.

76. Hrubý, A. Evaluation of glass-forming tendency by means of DTA. Czechoslovak Journal of Physics B 1972;22(11):1187-1193.

77. Thornburg, DD. Evaluation of glass formation tendency from rate dependent thermograms. Materials Research Bulletin 1974;9(11):1481-1485.

78. Mehta, N, Tiwari, RS, Kumar, A. Glass forming ability and thermal stability of some Se-Sb glassy alloys. Materials Research Bulletin 2006;41(9):1664-1672.

79. Tanaka, H. Relationship among glass-forming ability, fragility, and short-range bond ordering of liquids. Journal of Non-Crystalline Solids 2005;351(8):678-690.

80. Sebdani, MM, Mauro, JC, Smedskjaer, MM. Effect of divalent cations and SiO2 on the crystallization behavior of calcium aluminate glasses. Journal of Non-Crystalline Solids 2015;413:20-23.

81. Sebdani, MM, Mauro, JC, Jensen, LR, et al. Structure-property relations in calcium aluminate glasses containing different divalent cations and SiO2. Journal of Non-Crystalline Solids 2015;427:160-165.

82. Gong, J, Wu, J, Guan, Z. Examination of the indentation size effect in low-load vickers hardness testing of ceramics. Journal of the European Ceramic Society 1999;19(15):2625-2631.

83. Nix, WD, Gao, H. Indentation size effects in crystalline materials: A law for strain gradient plasticity. Journal of the Mechanics and Physics of Solids 1998;46(3):411-425.

84. Smedskjaer, MM. Topological Model for Boroaluminosilicate Glass Hardness. Frontiers in Materials 2014;1:23.

85. Smedskjaer, MM, Mauro, JC, Yue, YZ. Prediction of Glass Hardness Using Temperature-Dependent Constraint Theory. Physical Review Letters 2010;105(11).

86. Rouxel, T. Elastic Properties and Short-to Medium-Range Order in Glasses. Journal of the American Ceramic Society 2007;90(10):3019-3039.

87. Yoshida, S, Nishikubo, Y, Konno, A, et al. Fracture- and Indentation-Induced Structural Changes of Sodium Borosilicate Glasses. 2012.